Published by Institute of Physics Publishing for SISSA
Received: *March 30, 2008*
Accepted: *April 1, 2008*
Published: *April 14, 2008*

Geometrically induced phase transitions at large N

Jonathan J. Heckman and Cumrun Vafa

Jefferson Physical Laboratory, Harvard University,
Cambridge, MA 02138, U.S.A.
E-mail: jheckman@fas.harvard.edu, vafa@physics.harvard.edu

Abstract: Utilizing the large N dual description of a metastable system of branes and anti-branes wrapping rigid homologous S^2's in a non-compact Calabi-Yau threefold, we study phase transitions induced by changing the positions of the S^2's. At leading order in $1/N$ the effective potential for this system is computed by the planar limit of an auxiliary matrix model. Beginning at the two loop correction, the degenerate vacuum energy density of the discrete confining vacua split, and a potential is generated for the axion. Changing the relative positions of the S^2's causes discrete jumps in the energetically preferred confining vacuum and can also obstruct direct brane/anti-brane annihilation processes. The branes must hop to nearby S^2's before annihilating, thus significantly increasing the lifetime of the corresponding non-supersymmetric vacua. We also speculate that misaligned metastable glueball phases may generate a repulsive inter-brane force which stabilizes the radial mode present in compact Calabi-Yau threefolds.

Keywords: D-branes, Supersymmetry Breaking, Gauge-gravity correspondence, Flux compactifications.

JHEP04(2008)052

Contents

JHEP04(2008)052

1. Introduction

Metastable vacua of supersymmetric string and field theories possess the attractive feature that in contrast to a generic non-supersymmetric system, the underlying supersymmetry of the theory often provides better control over the dynamics of the vacuum. String theory realizations of metastable vacua have been discussed in [1 – 11]. Recent progress in finding non-supersymmetric metastable vacua in supersymmetric QCD-like field theories was achieved in [12] and subsequent string theory realizations of this work [13 – 27].

Combining these stringy insights with the dual closed string description of large N open string systems such as the AdS/CFT correspondence [28 – 30] and geometric transitions [1, 31, 32], it was shown in [6] that much of the rigid structure of $\mathcal{N} = 2$ supersymmetry remains intact for metastable vacua in type IIB string theory given by D5-branes and anti-D5-branes wrapping distinct minimal size S^2's in a non-compact Calabi-Yau geometry of the form:

$$y^2 = W'(x)^2 + uv \tag{1.1}$$

where $W'(x) = g(x-a_1)\cdots(x-a_n)$ is a polynomial of degree n, the variables $x, y, u, v \in \mathbb{C}$ and the minimal size S^2's are located at $x = a_i$. The a_i correspond to non-normalizable modes in the non-compact geometry which determine the relative separation between the branes. In the following we shall denote the number of branes (resp. anti-branes) by positive (resp. negative) integers. In the closed string dual description the branes (resp. anti-branes) wrapping S^2's are replaced by S^3's threaded by some amount of positive (resp. negative) RR flux. The geometry of the closed string dual description is given by blowing down the S^2 and introducing a complex deformation of equation (1.1) by a degree $n-1$ polynomial in x:

$$y^2 = W'(x)^2 + f_{n-1}(x) + uv \tag{1.2}$$

$$= g^2 \prod_{i=1}^{n} (x - a_i^+)(x - a_i^-) + uv. \tag{1.3}$$

This deformation splits the roots of $W'(x)^2$ to a_i^+ and a_i^- for all i and thus defines a Riemann surface with n branch cuts located near each of these roots.

At leading order in the $1/N$ expansion, the fluxes spontaneously break all of the $\mathcal{N} = 2$ supersymmetry of the Calabi-Yau compactification. Due to the fact that the moduli space is still governed by rigid special geometry, the matrix model techniques developed in [33 – 36] still determine all higher order corrections to the form of the periods in the closed string dual. In the open string description these higher order corrections correspond to multi loop contributions to the glueball potential. In [8] a rich phase structure for the two cut system was uncovered by including two loop corrections to the effective potential.

To frame some of the discussion to follow, we now review the two distinct ways in which the two cut system exhibits metastable behavior [8]. One decay mode is given by direct flux line annihilation where the domain wall delimiting the bubble of vacuum with lower flux is a stack of D5-branes wrapping the compact interpolating 3-cycle between the two S^3's supported by flux. See figure 1 for a depiction of this process. Two loop effects reveal

JHEP04(2008)052

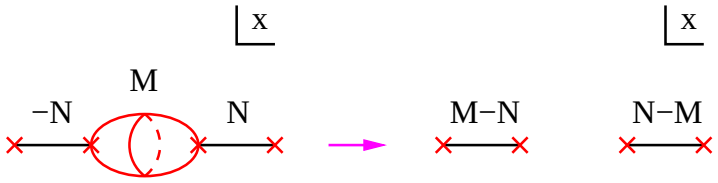

Figure 1: Depiction of flux line annihilation in a two cut geometry which initially consists of $N > 0$ units of flux through one cut and $-N$ through the other. In the depiction on the left, $M > 0$ D5-branes wrap the interpolating 3-cycle between the two S^3's supported by flux. In the Minkowski spacetime the stack of D5-branes separates a bubble of vacuum with flux numbers $(M - N, N - M)$ from one with flux numbers $(-N, N)$. The end of the annihilation process and the corresponding flux numbers are shown on the right.

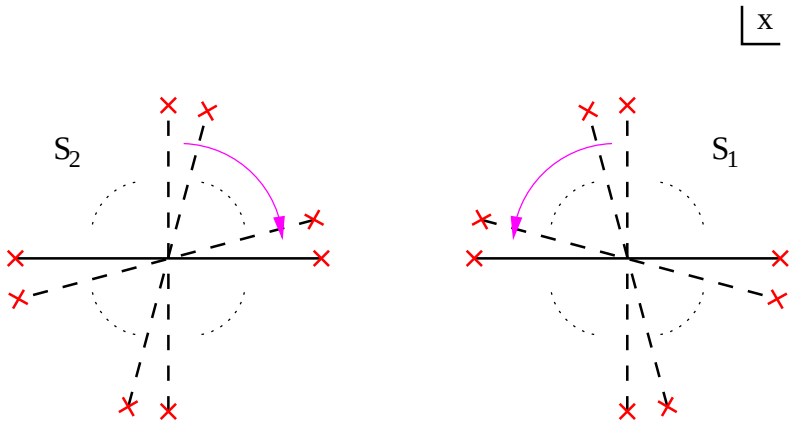

Figure 2: Two loop corrections to the glueball potential lift the degeneracy in energy density between the confining vacua of the theory. These vacua correspond to distinct orientations of the branch cuts in the closed string dual geometry. The metastable branch cut orientations denoted by dashed lines eventually decay to the energetically preferred configuration denoted by a solid line.

another way in which the vacua of the brane/anti-brane system are metastable. Whereas at one loop order the distinct confining vacua of the theory are energetically degenerate, beginning at two loop order this degeneracy is lifted. At large N and when the scale of confinement is not exponentially suppressed, the many confining vacua of the theory are all metastable. Geometrically, these vacua correspond to distinct orientations of the branch cuts. The decay to the lowest energy confining vacuum corresponds to a re-alignment of the branch cuts. See figure 2 for a depiction of this decay process.

Although the analysis of brane/anti-brane configurations with two minimal size S^2's should provide an adequate description of "two body"interactions, a generic compact Calabi-Yau threefold will typically contain a large number of rigid homologous S^2's which may also be wrapped by branes and anti-branes. For example, the quintic Calabi-Yau threefold contains 2875 rational curves of precisely this type. Perhaps surprisingly, we find that the presence of additional *unwrapped* S^2's introduces a further layer of phase structure.

As already mentioned in the two cut case, just as a supersymmetric configuration of

JHEP04(2008)052

N_i branes contains $Tr(-1)^F = N_1 \cdots N_n$ energetically degenerate confining vacua, at one loop order the vacua of the brane/anti-brane system also remain energetically degenerate. It follows from an analysis similar to the two cut case that the two loop contribution to the energy density lifts this degeneracy. We also find, however, that changing the location of the minimal size S^2's produces discrete jumps in the energetically preferred confining vacuum.

Interpreting the two loop energy density as a potential for the axion of our theory, we next study the minima of this potential as a function of the a_i's. We find that the presence of additional unwrapped S^2's contributes a moduli space of values such that the effective θ-angle of each brane theory relaxes to zero at the minimum of the axion potential. We next consider symmetric configurations where all S^2's are occupied and show that the discrete symmetries of the geometry translate into constraints on strong CP violation in brane/anti-brane configurations which remain invariant under the discrete symmetry $x \mapsto \overline{x}$.

Although a general analysis of the critical points of the n-cut system appears quite difficult using present techniques, to keep the analysis tractable we study configurations with $N_1 = N$ D5-branes and $N_2 = -N$ anti-D5-branes wrapping minimal size S^2's in a geometry defined by a collection of minimal size S^2's which all lie on the real axis and remain invariant under the map $x \mapsto -x$. We find that metastability is lost once the effective 't Hooft coupling becomes too large. At this point, the size of the corresponding branch cuts will begin to expand. A generic configuration of additional S^2's will typically obstruct a direct collision between the cuts supported by positive and negative flux. Such obstructions can lead to phase transitions to non-Kähler geometries of the type found in [8].

The additional S^2's can also obstruct direct brane/anti-brane annihilation. Utilizing the partial classification of BPS states of geometrically engineered $\mathcal{N} = 2$ gauge theories obtained in [37], we show that the presence of additional minimal size S^2's can sometimes cause the most efficient means of annihilation to proceed via a multi-domain wall process where a brane must first tunnel to an unoccupied minimal size S^2 before annihilating against an anti-brane.

Combining the analysis of the previous sections, we also briefly comment on the stabilization of the radial mode which is present in compact Calabi-Yau threefolds. Whereas the one loop contribution to the vacuum energy density generates a logarithmic Coulomb attraction term, the two loop contribution generates a power law contribution which is repulsive for appropriate glueball phases. Although suggestive, we find that the value of the radial mode is very close to the value which would destabilize the size of the glueball fields.

The rest of this paper is organized as follows. In section 2 we review the conjectured geometric transition for the brane/anti-brane system and briefly discuss the phase structure found in [8]. In this same section we also include a short discussion on the regime of string theory parameters for which we expect to have an accurate description of the low energy dynamics. In section 3 we compute the two loop contribution to the period matrix of the n-cut geometry. We briefly discuss the form of the effective potential for geometries with unoccupied S^2's in section 4. We next compute corrections to the vacuum energy density as well as constraints on axion potentials in sections 5 and 6, respectively. In section 7 we introduce a subclass of critical points in the presence of additional S^2's and study the breakdown of metastability in section 8. In section 9 we study brane/anti-brane

JHEP04(2008)052

annihilation processes and in section 10 we speculate on the stabilization of the radial mode. Section 11 presents our conclusions.

2. Geometrically induced metastability

In this paper we consider metastable vacua of type IIB string theory. More precisely, we study D5-branes and anti-D5-branes which fill Minkowski space and wrap n minimal size rigid homologous S^2's of a local Calabi-Yau threefold defined by the hypersurface of equation (1.1). This configuration is metastable because the tension of the branes creates a potential barrier against moving off of the minimal size S^2. We now review some further properties of this system, closely following the discussion in [6, 8]. At each point in the complex x-plane the area of the S^2 is:

$$A(x) = \left(\left|W'(x)\right|^2 + |r|^2\right)^{1/2} \tag{2.1}$$

where r denotes the stringy volume of the minimal size S^2's given by turning on a non-trivial NS B_2 field. The bare gauge coupling of the open string system is:

$$-\alpha\left(\Lambda_0\right) = \frac{4\pi i}{g_{\rm YM}^2} + \frac{\theta_{\rm YM}}{2\pi} = \frac{4\pi i}{g_s}\int_{S^2} B_2 + \int_{S^2} C_2 \tag{2.2}$$

where C_2 denotes the RR two form. In the large N limit, $N \to \infty$ but g_s scales as N^{-1} so that the associated 't Hooft coupling $g_s N$ remains finite.

In the holographic dual description, the branes and anti-branes wrapping n homologous S^2's of the original geometry are replaced by fluxes threading the n topologically distinct S^3's of the new geometry. The local Calabi-Yau threefold after the transition is defined by equation (1.2) where the coefficients of $f_{n-1}(x)$ correspond to the n normalizable complex deformation parameters of the Calabi-Yau. This complex equation defines a two-sheeted Riemann surface fibered over the u and v coordinates. See figure 3 for a depiction of this geometry.

The n S^3's correspond to n 3-cycles A_i such that $A_i \cap A_j = 0$ for all i, j. Dual to each A-cycle is a non-compact B-cycle such that $A_i \cap B_j = -B_j \cap A_i = \delta_{ij}$ and $B_i \cap B_j = 0$ for all i, j. At the level of the Riemann surface, the A_i reduce to n distinct counterclockwise contours encircling each of the n branch cuts of the Riemann surface and the B_i reduce to contours which extend from the point $x = \Lambda_0$ on the lower sheet to the point $x = \Lambda_0$ on the upper sheet. The IR cutoff defined by Λ_0 in the geometry is identified with a UV cutoff in the open string description. The periods of the holomorphic three form Ω along the cycles A_i and B_i define a basis of special coordinates for the complex structure moduli space:

$$S_i = \int_{A_i} \Omega, \qquad \Pi_i = \frac{\partial \mathcal{F}_0}{\partial S_i} = \int_{B_i} \Omega \tag{2.3}$$

where $\mathcal{F}_0$ denotes the genus zero prepotential. In the absence of fluxes, each S_i corresponds to the scalar component of a $\mathrm{U}(1)$ $\mathcal{N} = 2$ vector multiplet. Once branes are introduced,

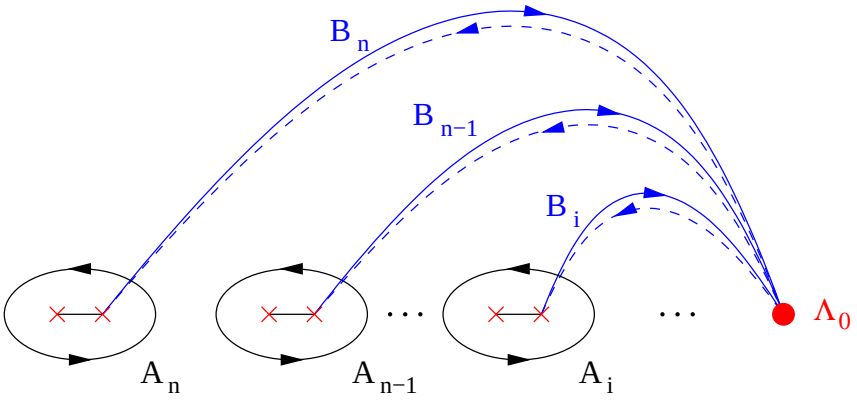

Figure 3: Depiction of the complex x-plane corresponding to the Riemann surface defined by equation (1.2) with $uv = 0$. The compact A-cycles reduce to counterclockwise contours which encircle each of the n branch cuts of the Riemann surface. The non-compact B-cycles reduce to contours which extend from $x = \Lambda_0$ on the lower sheet (dashed lines) to $x = \Lambda_0$ on the upper sheet (solid lines).

each S_i is identified in the open string description with the size of a gaugino condensate. Defining the period matrix:

$$\tau_{ij} = \frac{\partial \Pi_i}{\partial S_j} = \frac{\partial^2 \mathcal{F}_0}{\partial S_i \partial S_j}, \tag{2.4}$$

to leading order in the $1/N$ expansion, the Kähler metric for the effective field theory is $\mathrm{Im}\,\tau_{ij}$. For future use we also introduce the Yukawa couplings:

$$\mathcal{F}_{ijk} \equiv \frac{\partial^3 \mathcal{F}_0}{\partial S_i \partial S_j \partial S_k}. \tag{2.5}$$

The net three form flux after the system undergoes a geometric transition is:

$$H_3 = H_{\mathrm{RR}} + \tau_{\mathrm{IIB}} H_{\mathrm{NS}} \tag{2.6}$$

where H_{RR} is the net RR three form field strength, H_{NS} is the net NS three form field strength and $\tau_{\mathrm{IIB}} = C_0 + ie^{-\phi}$ is the type IIB axio-dilaton. Explicitly,

$$N_i = \int_{A_i} H_3, \qquad \alpha = \alpha_i = -\int_{B_i} H_3 \tag{2.7}$$

for all i. Assuming that the fluxes spontaneously break the $\mathcal{N} = 2$ supersymmetry of the system, the flux induced effective potential is [6]:

$$V_{\mathrm{eff}} = \left(\alpha_k + N^{k'}\tau_{k'k}\right)\left(\frac{1}{\mathrm{Im}\,\tau}\right)^{kl}\left(\overline{\alpha}_l + \overline{\tau}_{ll'}N^{l'}\right) + \frac{8\pi}{g_{\mathrm{YM}}^2}\left(N_1 + \cdots + N_n\right) \tag{2.8}$$

where we have introduced a constant shift in order to properly compare the tension of branes and anti-branes [6]. Near the conifold point the entries of the τ matrix satisfy:

$$2\pi i \tau_{ij} = \delta_{ij} \log \frac{S_i}{W^{(2)}(a_i)\Lambda_0^2} - (1 - \delta_{ij}) \log \frac{\Lambda_0^2}{\Delta_{ij}^2} + f_{ij}\left(S_1, \ldots, S_n\right) \tag{2.9}$$

JHEP04(2008)052

where δ_{ij} denotes the Kronecker delta, $\Delta_{ij} = a_i - a_j$ and f_{ij} denotes an analytic power series in the variables S_i. The degree l terms in f_{ij} correspond to the $l+1$ loop contribution to the period matrix in the low energy effective theory.

Letting B denote the set of branes and $\overline{B}$ the set of anti-branes, the critical points of the one loop effective potential satisfy [6]:

$$\alpha + \sum_{j\in B} \tau_{ij} N_j + \sum_{j\in\overline{B}} \overline{\tau_{ij}} N_j = 0 \tag{2.10}$$

with vacuum energy density:

$$E^{(0)} = \frac{8\pi}{g_{\rm YM}^2}\left(\sum_{i\in B}|N_i| + \sum_{j\in\overline{B}}|N_j|\right) - \frac{2}{\pi}\sum_{i\in B, j\in\overline{B}}|N_i|\,|N_j|\log\left|\frac{\Lambda_0}{\Delta_{ij}}\right|^2. \tag{2.11}$$

Solving for the glueball fields yields:

$$S_i = \zeta_i W^{(2)}(a_i)\Lambda_0^2 \prod_{i\neq j\in B}\left(\frac{\Lambda_0}{\Delta_{ij}}\right)^{2\left|\frac{N_j}{N_i}\right|} \prod_{k\in\overline{B}}\left(\frac{\overline{\Lambda_0}}{\overline{\Delta_{ik}}}\right)^{2\left|\frac{N_k}{N_i}\right|} \exp\left(-\frac{2\pi i\alpha\,(\Lambda_0)}{|N_i|}\right) \qquad (N_i > 0) \tag{2.12}$$

$$S_i = \zeta_i W^{(2)}(a_i)\Lambda_0^2 \prod_{i\neq k\in\overline{B}}\left(\frac{\Lambda_0}{\Delta_{ik}}\right)^{2\left|\frac{N_k}{N_i}\right|} \prod_{j\in B}\left(\frac{\overline{\Lambda_0}}{\overline{\Delta_{ij}}}\right)^{2\left|\frac{N_j}{N_i}\right|} \exp\left(\frac{2\pi i\overline{\alpha}\,(\Lambda_0)}{|N_i|}\right) \qquad (N_i < 0) \tag{2.13}$$

where ζ_i denotes an $|N_i|^{\rm th}$ root of unity. These discrete phase choices label the distinct confining vacua of the theory.

As explained in greater detail in [6], the brane/anti-brane system decays to the supersymmetric ground state by nucleating a bubble of lower vacuum energy density. The corresponding domain wall solution is given by a D5-brane wrapping a supersymmetric 3-chain in the Calabi-Yau threefold. From the perspective of the closed string dual, the D5-brane wrapping the corresponding supersymmetric 3-cycle separates vacua with different amounts of flux quanta.

The type IIA T-dual description of the brane/anti-brane system with two minimal size S^2's was first commented on in [18] and studied in detail in [11]. This corresponds to a configuration with D4-branes and anti-D4-branes suspended between a pair of NS5-branes defined by the equations $y = \pm W'(x)$. The analogue of the IIB closed string description maps to the regime where the D4-branes and anti-D4-branes have dissolved as flux in the NS5-branes. This configuration was also lifted to an M-theory description given by an M5-brane wrapping a harmonic rather than holomorphic curve. As noted in [11], although the absence of supersymmetry would seemingly preclude any direct connection between the effective potentials of the IIB and IIA systems due to the difference in the size of the T-dualized circle, the observed match in the limit $g_s \to 0$ between the two effective potentials provides further evidence that at leading order in the $1/N$ expansion supersymmetry is indeed spontaneously broken by the presence of fluxes.

JHEP04(2008)052

Due to the fact that a convenient parametrization of the associated M-theory curve is not known for n-cut geometries, we will unfortunately not be able to exploit the powerful techniques developed in [11] to describe the $g_s \to 0$ limit of the all loop phase structure of the associated system for even a restricted set of fluxes.

Before proceeding to a short review of the two cut phase structure, we first comment on the possibility of additional corrections to the Kähler potential due to α' corrections. This is a subtle point because in order to keep the string modes which mediate supersymmetry breaking from decoupling we must keep α' finite. Although in the strict infinite volume limit such effects will apparently not alter the form of the Kähler potential, for finite Kähler modulus such corrections will introduce important corrections [38]. Because we work in the context of non-compact Calabi-Yau threefolds, we shall assume for the purposes of this paper that such corrections are negligible.

2.1 Two cut phase structure

We now review the phase structure of the two cut system [8]. At leading order in an expansion of the periods, the two cut period matrix is [39]:

$$2\pi i\tau = \begin{pmatrix} \log\frac{S_1}{g\Delta_{12}\Lambda_0^2} & -\log\frac{\Lambda_0^2}{\Delta_{12}^2} \\ -\log\frac{\Lambda_0^2}{\Delta_{12}^2} & \log\frac{S_2}{-g\Delta_{12}\Lambda_0^2} \end{pmatrix} \tag{2.14}$$

$$+ \begin{pmatrix} 4\frac{S_1}{g\Delta_{12}^3} - 10\frac{S_2}{g\Delta_{12}^3} & -10\frac{S_1}{g\Delta_{12}^3} + 10\frac{S_2}{g\Delta_{12}^3} \\ -10\frac{S_1}{g\Delta_{12}^3} + 10\frac{S_2}{g\Delta_{12}^3} & -4\frac{S_2}{g\Delta_{12}^3} + 10\frac{S_1}{g\Delta_{12}^3} \end{pmatrix} + \mathcal{O}\left(S^2\right). \tag{2.15}$$

As shown in [8], there is an intricate phase structure beginning at two loop order. Just as a supersymmetric configuration of N_i branes contains $Tr(-1)^F = N_1 N_2$ energetically degenerate confining vacua, at one loop order the confining vacua of the brane/anti-brane system also remain energetically degenerate. These vacua correspond to the different roots of unity appearing in the one loop critical points of equations (2.12) and (2.13). Beginning at two loop order, this degeneracy in the energy densities is lifted. In the closed string dual, the confining vacuum of lowest energy corresponds to a configuration where the branch cuts align along a common axis in the complex x-plane. When the size of the confinement scale is fixed to a finite value, the action for quantum tunneling to the energetically preferred confining vacuum scales as a positive power of N so that the corresponding tunneling rate is exponentially suppressed. The two loop contribution to the effective potential also destabilizes the vacuum once the flux becomes comparable to the value:

$$g_{\rm YM}^2 N \sim \frac{1}{\log\left|\frac{\Lambda_0}{\Delta_{12}}\right|}. \tag{2.16}$$

Once metastability is lost, the branch cuts begin to expand until they nearly collide. When this occurs the interpolating 3-cycle $B_1 - B_2$ collapses to nearly zero size. The contribution due to additional light states can potentially drive the system to two qualitatively different endpoints. Whereas D5-branes wrapping $B_1 - B_2$ will tend to lower the flux of the

JHEP04(2008)052

corresponding configuration so that the system relaxes back to another metastable configuration, the contribution due to a D3-brane wrapping the same collapsing cycle can trigger a transition to a non-Kähler geometry [8].

3. Matrix model computation

In order to study the phase structure of more general geometries, we first determine the two loop contribution to the period matrix in the n-cut geometry. Although it is in principle possible to determine the form of this correction by directly evaluating the period integrals of the closed string dual, we shall instead use the matrix model technology developed in [33 – 35] to reduce the computation to a perturbative Feynman diagram analysis. This will have the added benefit that we will be able to isolate individual string exchange processes which contribute to the vacuum energy density.

The genus zero prepotential of the closed string dual geometry is computed to all orders by the planar limit of a large N auxiliary matrix model with partition function:

$$Z_{MM} = \frac{1}{\mathrm{Vol}\left(U\left(N\right)\right)} \int d\Phi \exp\left(-\frac{1}{g_s} Tr W\left(\Phi\right)\right) \tag{3.1}$$

where Φ is a holomorphic $N \times N$ matrix and the above matrix integral should be understood as a contour integral. The prepotential of the n-cut geometry near the semi-classical expansion point is given by expanding the eigenvalues of Φ about the n critical points of the polynomial W. The usual eigenvalue repulsion term of the matrix model causes these eigenvalues to fill the n cuts of the geometry after the geometric transition. With M_i eigenvalues sitting at the i^{th} cut of the geometry, this matrix model may be recast as an n-matrix model of the form:

$$Z_{MM} = \frac{1}{\prod_{i=1}^{n} \mathrm{Vol}\left(U\left(M_i\right)\right)} \int d\Phi_{11} \cdots d\Phi_{nn} \exp\left(\sum_{i=1}^{n} - \frac{1}{g_s} W_i\left(\Phi_{ii}\right) - \frac{1}{g_s} W_{\mathrm{int}}\left(\Phi_{11}, \ldots, \Phi_{nn}\right)\right) \tag{3.2}$$

where Φ_{ii} denotes the $M_i \times M_i$ block of Φ along its diagonal. The periods of the A-cycles are given by the partial 't Hooft couplings of the matrix model:

$$S_i = g_s M_i. \tag{3.3}$$

Evaluating Z_{MM} in the saddle point approximation, the genus zero prepotential is:

$$\mathcal{F}_0 = \mathcal{F}_{\mathrm{non-pert}} + \mathcal{F}_{\mathrm{pert}} \tag{3.4}$$

where $\mathcal{F}_{\mathrm{non-pert}}$ corresponds to contributions from the $\mathrm{Vol}(U\left(M_i\right))$ factors and $\mathcal{F}_{\mathrm{pert}}$ corresponds to the perturbative contributions from planar Feynman diagrams:

$$2\pi i \mathcal{F}_{\mathrm{non-pert}} = \sum_{i=1}^{n} \frac{1}{2} S_i^2 \log \frac{S_i}{\Lambda_0^3} \tag{3.5}$$

$$2\pi i \mathcal{F}_{\mathrm{pert}} = \sum_{i=1}^{n} - S_i W(a_i) + \sum_{0 \leq i_1, \ldots, i_n} C_{i_1 \ldots i_n} S_1^{i_1} \cdots S_n^{i_n} \tag{3.6}$$

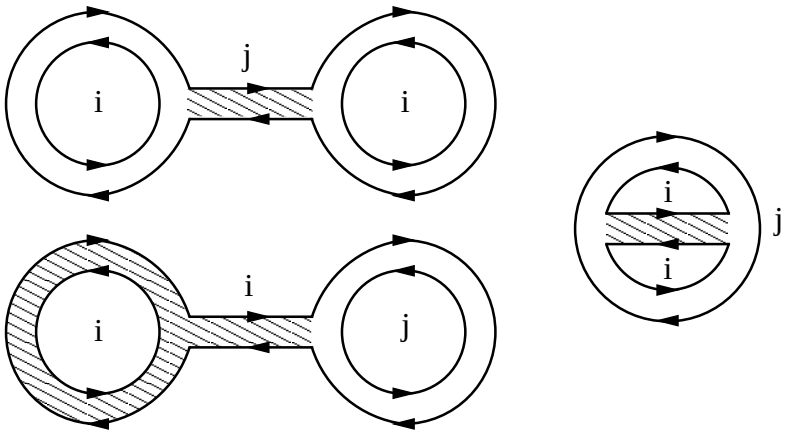

Figure 4: Depiction of all Feynman diagrams which contribute to the $M_i^2 M_j$ term of $\mathcal{F}_{\rm pert}$ for $i \neq j$. In each diagram, ghost propagators are denoted by white and Φ propagators by dashed lines. The index loops of each diagram are also shown.

where the $C_{i_1 \ldots i_n}$ are coefficients which are in principle calculable.

We now compute all contributions to $\mathcal{F}_{\rm pert}$ proportional to $M_i M_j M_k$ for all i, j, k. Following [36], the gauge-fixed matrix model action is given by the sum of two contributions:

$$S_{\rm MM} = S_\Phi + S_{\rm ghost} \tag{3.7}$$

where:

$$S_\Phi = \frac{1}{g_s} \sum_{r \geq 0} \sum_i \frac{W^{(r)}(a_i)}{r!} Tr\left(\Phi_{ii}\right)^r \tag{3.8}$$

and:

$$S_{\rm ghost} = \frac{1}{g_s} \sum_{i \neq j} Tr\left(\Delta_{ji} B_{ij} C_{ji} + B_{ij} \Phi_{jj} C_{ji} + C_{ij} \Phi_{jj} B_{ji}\right) \tag{3.9}$$

where C_{ij} denotes a scalar ghost and B_{ij} its conjugate. In the above we have also introduced a constant shift in the definition of the Φ_{ii}'s. Suppressing all matrix indices, the propagators of the fields are:

$$\langle \Phi_{ii} \Phi_{ii} \rangle = \frac{g_s}{W^{(2)}(a_i)} \tag{3.10}$$

$$\langle B_{ij} C_{ji} \rangle = \frac{g_s}{\Delta_{ij}} \tag{3.11}$$

for all $i \neq j$. The l-point interaction vertex of l Φ_{ii} fields has weight $-W^{(l)}(a_i)/g_s(l-1)!$ and the three point interaction vertex between the B, C and Φ fields has weight $-1/g_s$.

For $i \neq j$, the three Feynman diagrams which contribute to the $M_i^2 M_j$ term of the free energy are depicted in figure 4. Proceeding from the right-most diagram to the upper left diagram in a clockwise direction, the contribution of each diagram to the matrix model free energy is:

$$A_{iij} = -\frac{g_s M_i^2 M_j}{W^{(2)}(a_i) \Delta_{ij}^2} - \frac{g_s M_i^2 M_j W^{(3)}(a_i)}{W^{(2)}(a_i)^2 \Delta_{ij}} + \frac{2 g_s M_i^2 M_j}{W^{(2)}(a_j) \Delta_{ij}^2}. \tag{3.12}$$

For $i \neq j \neq k \neq i$, the diagrams which contribute to the $M_i M_j M_k$ term of the free energy possess the same ghost and Φ field content as the upper left diagram of figure 4 but with all three index loops distinct. The net contribution to the matrix model free energy from this class of diagrams is:

$$A_{ijk} = \frac{4 g_s M_i M_j M_k}{W^{(2)}(a_i)\Delta_{ij}\Delta_{ik}} + (i \leftrightarrow j) + (i \leftrightarrow k). \tag{3.13}$$

Two of the three diagrams which contribute to the M_i^3 term of the free energy are given by replacing the ghost content of the diagrams of figure 4 by Φ fields and interaction vertices. When three or more cuts are present, a planar figure eight diagram also contributes. Starting from the right-most diagram of figure 4 and ending with the figure eight diagram, the net contribution to the matrix model free energy from this class of diagrams is:

$$A_{iii} = \frac{g_s M_i^3 W^{(3)}(a_i)^2}{24 W^{(2)}(a_i)^3} + \frac{g_s M_i^3 W^{(3)}(a_i)^2}{8 W^{(2)}(a_i)^3} - \frac{g_s M_i^3 W^{(4)}(a_i)}{12 W^{(2)}(a_i)^2}. \tag{3.14}$$

The two loop corrections to the period matrix are summarized in appendix A.

4. Effective potentials and unoccupied S^2's

In this brief section we explain how to treat the effective potential for brane/anti-brane systems with unoccupied minimal size S^2's. To this end, we first review the treatment of similar supersymmetric brane configurations developed in [40]. Due to the fact that all of the initial S^2's in the open string description are homologous, even an unwrapped S^2 will naïvely undergo a geometric transition to an S^3. Note, however, that because there is no flux to support the S^3 counterparts of the unwrapped S^2's, additional light degrees of freedom corresponding to D3-branes wrapping the collapsing S^3's will enter the low energy dynamics. The effective superpotential now includes contributions of the form:

$$\alpha S + \sqrt{2} Q_L Q_R S \subset \mathcal{W}_{\text{eff}} \tag{4.1}$$

where Q_L and Q_R denote two $\mathcal{N} = 1$ chiral multiplets which combine to form the $\mathcal{N} = 2$ hypermultiplet describing the D3-brane. When the Q fields condense, the original S^3 disappears and is replaced by an S^2 of size $\langle Q_L Q_R \rangle = -\alpha/\sqrt{2}$. The glueball superpotential for such a system is computed by a matrix model with action given by $W(x)$ where the S_i's corresponding to zero flux are set to zero in the prepotential.

In the non-supersymmetric brane/anti-brane configurations studied in this paper, the effective potential is controlled by the period matrix τ_{ij}. Due to the fact that $\mathcal{N} = 2$ supersymmetry is spontaneously broken at leading order in $1/N$ by the presence of positive and negative flux, the prescription for supersymmetric configurations described above will continue to hold in the non-supersymmetric context. Labelling the fluxes so that $N_1, \ldots, N_l \neq 0$ for some positive integer $l \leq n$ with all other N_i equal to zero, the appropriate period matrix to use in equation (2.8) is given by the $l \times l$ truncation of τ_{ij} to $1 \leq i, j \leq l$ where all glueball fields corresponding to zero flux have been formally set to zero in the prepotential.

JHEP04(2008)052

5. Two loop corrections to the energy density

At one loop order, equation (2.11) implies that the discrete phase choices for the glueball fields present in equations (2.12) and (2.13) have identical vacuum energy densities. As in the two cut case, we find that two loop effects lift this degeneracy. The decay to the confining vacuum of lowest energy proceeds via D5-branes wrapping the A-cycles in the closed string dual geometry. We refer the reader to [8] for further discussion on the alignment of glueball phases due to tunneling processes. In this section we study the orientation of the branch cuts in the lowest energy confining vacuum as a function of the roots of $W'(x)$.

In the remainder of this paper we let $\delta\tau$ denote the two loop correction to the period matrix. Expanding V_{eff} to linear order in $\delta\tau$ and applying equation (2.10) yields the first order correction to the vacuum energy density due to two loop effects:

$$E = E^{(0)} + \sum_{j\in B, k\in \overline{B}} 4\,|N_j|\,|N_k|\,\mathrm{Re}\,(i\delta\tau_{jk}) + \mathcal{O}(\delta\tau^2) \tag{5.1}$$

where $\delta\tau_{jk}$ is evaluated at the one loop corrected value of the S_i's given by equations (2.12) and (2.13). In the following we shall refer to the second term as δE. Because the components of $\delta\tau_{jk}$ are linear in the S_i's, we conclude that the two loop contribution lifts the degeneracy in energy present at one loop order. Note in particular that the energy only receives contributions from off-diagonal brane/anti-brane components of $\delta\tau_{jk}$.

From the perspective of the closed string dual geometry, the phases of the S_i's correspond to the direction of alignment for the branch cuts in the complex x-plane. Expanding the defining period integrals for the S_i in terms of $\left(a_i^+ - a_i^-\right)$ yields:

$$S_i = \frac{g}{2\pi i}\int_{a_i^-}^{a_i^+} \sqrt{\prod_{i=1}^{n}(x-a_i^+)(x-a_i^-)}dx = \frac{1}{4}W^{(2)}(a_i)\,(\delta x_i)^2 + \mathcal{O}(\delta x^3) \tag{5.2}$$

where $4\,(\delta x_i)^2 = (a_i^+ - a_i^-)^2$.

Although there is an ambiguity in the sign of the above period integral due to the presence of the square root, the different choices of signs correspond to distinct orientations of the A- and B- cycles in the Calabi-Yau threefold. Indeed, once the orientation of the B-cycles is fixed, the choice of signs in the above period integrals are then completely fixed. To determine the appropriate sign, we consider a geometry given by branch cuts which are all located on the real axis of the complex x-plane with $g, \Lambda_0 > 0$. Ordering the points so that $a_1^+ > a_1^- > \cdots > a_n^+ > a_n^-$, we have:

$$\Pi_1 = \frac{g}{2\pi i}\int_{a_1^+}^{\Lambda_0} \sqrt{\prod_{i=1}^{n}(x-a_i^+)(x-a_i^-)}dx = \frac{R}{2\pi i} \tag{5.3}$$

where R is a real number. Adhering to the sign conventions used in [39], general monodromy arguments yield:

$$\Pi_1 \sim \frac{S_1}{2\pi i}\log\frac{S_1}{W^{(2)}(a_1)\Lambda_0^2} + \mathcal{O}(S^0). \tag{5.4}$$

We therefore conclude that the proper choice of sign for S_1 and therefore all of the S_i's is the one given by equation (5.2).

In the rest of this section we study the alignment of branch cuts in the lowest energy confining vacuum. Because there are a discrete number of confining vacua, a generic change in the parameters a_i will typically induce a small jump of $\mathcal{O}(1/N)$ in the preferred confining vacuum. At large N such small jumps do not produce a dramatic change in the physics because we already approximate the discrete phase choice by a continuous variable. Even in this limit, however, we find that an appropriate variation of parameters can induce large discrete jumps in the preferred confining vacuum. In subsection 5.1 we treat geometries with three minimal size S^2's and present two examples where the alignment of cuts naturally generalizes the results found for two cut geometries. We next demonstrate that for more general configurations, changing the relative positions of the a_i's can induce discrete jumps in the preferred alignment direction of the branch cuts. In subsection 5.2 we generalize this analysis to configurations with additional minimal size S^2's.

5.1 Alignment with three minimal S^2's

We now study the energetics of branch cut alignment in geometries with:

$$W'(x) = g(x-a_1)(x-a_2)(x-a_3). \tag{5.5}$$

Our expectation is that configurations with a high degree of symmetry will exhibit behavior which is similar to that of the two cut system.

As a first example, we take the a_i's to form an equilateral triangle with $N_1 > 0$ D5-branes at $x = a_1 = a$, $N_2 > 0$ D5-branes at $x = a_2 = -a$, and $N_3 < 0$ anti-D5-branes at $x = a_3 = i\sqrt{3}a$. Setting $\delta x_i = r_i e^{i\beta_i}$ with $r_i > 0$, the two loop contribution to the energy is given by the second term of equation (5.1):

$$\delta E = \mathrm{Re}\left[\begin{array}{c} \frac{|N_1||N_3|}{8\pi a^2}\left(-1-7i\sqrt{3}\right) r_1^2 e^{2i\beta_1} + \frac{|N_2||N_3|}{8\pi a^2}\left(-1+7i\sqrt{3}\right) r_2^2 e^{2i\beta_2} \\ +\left(\frac{|N_1||N_3|}{8\pi a^2}\left(11-3i\sqrt{3}\right) + \frac{|N_2||N_3|}{8\pi a^2}\left(11+3i\sqrt{3}\right)\right) r_3^2 e^{2i\beta_3} \end{array}\right]. \tag{5.6}$$

Minimizing δE with respect to the β_i's, it now follows that in the lowest energy configuration the cuts always point towards the interior of the triangle. Bisecting each 60° angle of the equilateral triangle, we further find that the cuts threaded by positive flux align on the side of the bisection closest to the cut with negative flux. Finally, it follows from the last line of equation (5.6) that the orientation of the cut with negative flux depends on the relative magnitudes of $|N_1|$ and $|N_2|$.

In fact, the position of minimal size S^2's not wrapped by branes will also influence the alignment of the cuts in the lowest energy confining vacuum. To this end, consider a configuration with $N_1 > 0$ D5-branes located at $x = a_1 = a > 0$, $N_2 < 0$ anti-D5-branes located at $x = a_2 = -a$ and with a vanishingly small number of branes or anti-branes wrapping the S^2 at $x = a_3 = c$. In this case $(\delta x_3)^2 = 0$ and the correction δE takes the form:

$$\delta E = \frac{|N_1|\,|N_2|}{4\pi a^2}\,\mathrm{Re}\left(\left(-5-\frac{8ac}{a^2-c^2}\right)(\delta x_1)^2 + \left(-5+\frac{8ac}{a^2-c^2}\right)(\delta x_2)^2\right). \tag{5.7}$$

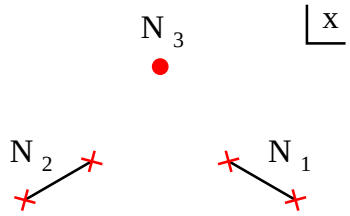

Figure 5: Depiction of branch cut orientation in the lowest energy confining vacuum of the three cut system with $N_1 > 0$ units of flux through the cut near $x = a$, $N_2 < 0$ units of flux through the cut near $x = -a$ and $N_3 = 0$ units of flux through the cut near $x = iL$ with $L, a > 0$. The presence of the additional minimal size S^2 at $x = iL$ causes the two cuts supported by flux to tip up.

Note that in the limit $c \to \infty$,

$$\lim_{c\to\infty} \delta E = -\frac{5\,|N_1|\,|N_2|}{4\pi a^2}\,\mathrm{Re}\left((\delta x_1)^2 + (\delta x_2)^2\right) \tag{5.8}$$

the corresponding S^2 at $x = c$ decouples from the dynamics of the theory and we find that just as in the two cut geometry, the branch cuts align with the real axis of the complex x-plane in the minimal energy configuration.

The symmetries of such configurations still constrain the direction of alignment. Indeed, when the a_i's form an isosceles triangle with $c = iL$ a pure imaginary number, we find:

$$\delta E = \frac{|N_1|\,|N_2|}{\pi}\,\mathrm{Re}\left(Q r_1^2 e^{2i\beta_1} + \overline{Q} r_2^2 e^{2i\beta_2}\right) \tag{5.9}$$

where $\delta x_i = r_i e^{i\beta_i}$ and Q is a complex number. It thus follows that the system has lowest energy when $\beta_1 = -\beta_2$ so that the branch cuts point symmetrically towards $x = c$. Indeed, expanding equation (5.7) for small L/a yields:

$$\delta E = -\frac{5\,|N_1|\,|N_2|}{4\pi a^2}\,\mathrm{Re}\left(e^{8iL/5a} r_1^2 e^{2i\beta_1} + e^{-8iL/5a} r_2^2 e^{2i\beta_2}\right) + \mathcal{O}\left(\frac{L^2}{a^2}\right) \tag{5.10}$$

so that both cuts tip towards $x = c$ with angle $4L/5a$. Although the cuts tip so as to touch one another, they do not align at the proper angle to touch the point $x = c$. This indicates that when all three cuts are of finite size, the energetically preferred configuration corresponds to the case where the endpoints of the cuts are maximally close to touching.

The above examples suggest that although the alignment of the branch cuts in the minimal energy confining vacuum depends on the roots of $W'(x)$, up to small discrete jumps of order $1/N$, this alignment is a smooth function of the relative position of the a_i's. Indeed, the coefficients multiplying $(\delta x_i)^2$ are rational functions of the a_i. Note, however, that varying the a_i will produce a discrete jump in the alignment of the branch cuts whenever crossing through the zero set of this rational function. When the position of a single root of a_i is varied, this zero set reduces to a finite number of points in the complex x-plane. In this case a jump can be avoided by traversing a contour which does not pass through such a root.

To establish the existence of such jumping phenomena, we restrict to configurations where all three a_i's lie on the real axis of the complex x-plane and $N_1 > 0 > N_2$, and N_3 is vanishingly small. With notation as in the previous example, the branch cuts in the minimal energy confining vacuum align parallel to the real axis when c lies within the union of the following intervals:

$$c \in (-\infty, -a) \cup \left(\frac{a}{5}\left(4-\sqrt{41}\right), a\right) \cup \left(\frac{a}{5}\left(4+\sqrt{41}\right), \infty\right) \qquad \Rightarrow \delta x_1 \in \mathbb{R} \qquad (5.11)$$

$$c \in \left(-\infty, -\frac{a}{5}\left(4+\sqrt{41}\right)\right) \cup \left(-a, \frac{a}{5}\left(-4+\sqrt{41}\right)\right) \cup (a, \infty) \qquad \Rightarrow \delta x_2 \in \mathbb{R} \qquad (5.12)$$

and perpendicular to the real axis for all other values of $c \in \mathbb{R}$ which do not cause the coefficients of $(\delta x_i)^2$ to vanish. Hence, there exist regions on the real line where both cuts are parallel, and one is parallel while the other is perpendicular to the real axis of the complex x-plane. Due to the fact that for $g > 0$, $W^{(2)}(a)$ is positive for $c < a$ and negative for $c > a$ we conclude that the glueball phases are also sensitive to the location of the unoccupied S^2.

Although the locations in the complex x-plane where cut alignment phase transitions occur appear to have little geometric content, the individual string exchange diagrams determined by the matrix model reflect the underlying location of the D5-branes and anti-D5-branes in the open string description. Without loss of generality, we focus on the contributions to the alignment of the cut near $x = a_1 = a$. Proceeding from the right-most diagram to the upper lefthand diagram in a clockwise direction in figure 4, the sign of the contribution of each diagram to the alignment of δx_1 along the real axis of the complex x-plane is:

$$sign\left(-\frac{1}{W^{(2)}(a_1)}\frac{1}{\Delta_{12}^2}W^{(2)}(a_1)\right) \Rightarrow \delta x_1 \in \mathbb{R} \qquad \text{for } c \in \mathbb{R} \qquad (5.13)$$

$$sign\left(-\frac{W^{(3)}(a_1)}{W^{(2)}(a_1)^2}\frac{1}{\Delta_{12}}W^{(2)}(a_1)\right) \Rightarrow \delta x_1 \in \mathbb{R} \qquad \text{for } c \notin [a_1, a_1+\Delta_{12}] \qquad (5.14)$$

$$sign\left(\frac{2}{W^{(2)}(a_2)}\frac{1}{\Delta_{12}^2}W^{(2)}(a_1)\right) \Rightarrow \delta x_1 \in \mathbb{R} \qquad \text{for } c \notin [a_2, a_1]\,. \qquad (5.15)$$

Note in particular that for the second $1-2$ exchange diagram the alignment of the cut depends on the location of an "image charge"at $x = a_1 + \Delta_{12}$. There is a final class of $2-3$ string exchange diagrams which can also contribute to the alignment of δx_1 when $N_3 > 0$. These correspond to diagrams with the same shape as in the upper lefthand diagram of figure 4, but with all index loops distinct. In this case all three diagrams contribute with the same sign to the alignment of δx_1 along the real axis:

$$sign\left(\frac{4}{W^{(2)}(a_1)\,\Delta_{12}\Delta_{13}}W^{(2)}(a_1)\right) \Rightarrow \delta x_1 \in \mathbb{R} \qquad \text{for } c > a_1. \qquad (5.16)$$

The above analysis indicates that the sign of each string exchange diagram depends only on whether c falls to the left or right of $x = a_2$ and $x = a_1$. Indeed, the classical trajectories of the string exchange processes in the complex x-plane sometimes must bend in order to avoid passing too close to the S^2 at $x = c$.

JHEP04(2008)052

5.2 Alignment with multiple minimal S^2's

We now extend the analysis of the previous subsection to configurations where $W'(x)$ has multiple roots. Although it is tempting to speculate based on the examples of the previous subsection that a large discrete jump in the preferred alignment direction of a branch cut will not occur in highly symmetric configurations, in this subsection we show that even when the roots of $W'(x)$ appear symmetrically along the real axis of the complex x-plane, the orientation of the cuts in the lowest energy configuration still suffers discrete jumps.

Most generally, we have:

$$W'(x) = g(x^2 - a^2)f(x) \tag{5.17}$$

where $f(x)$ is a monic polynomial with isolated roots. With $N_1 > 0$ D5-branes located at $x = a > 0$ and $N_2 < 0$ anti-D5-branes at $x = -a$ with a vanishingly small number at the remaining roots of $W'(x)$, the two loop contribution to the energy density is:

$$\delta E = \frac{|N_1|\,|N_2|}{4\pi a^2}\,\mathrm{Re}\left(\begin{array}{c}\left(-3 - 2\prod_{i=1}^{m}\frac{c_i - a}{a + c_i} - \sum_{i=1}^{m}\frac{4a}{a - c_i}\right)(\delta x_1)^2 \\ +\left(-3 - 2\prod_{i=1}^{m}\frac{a + c_i}{c_i - a} - \sum_{i=1}^{m}\frac{4a}{a + c_i}\right)(\delta x_2)^2\end{array}\right) \tag{5.18}$$

where $c_1, \ldots, c_m$ denote the roots of $f(x)$. Treating the c_i as m complex coordinates in $\mathbb{C}^m$, note that the coefficients multiplying $(\delta x_1)^2$ and $(\delta x_2)^2$ both vanish on complex manifolds of dimension $m - 1$. It follows that crossing this zero set will induce a jump in the branch cut orientation of the energetically preferred confining vacuum.

Although an analysis indicating the various phase regions for cut alignment for general c_i will likely be complicated, when a higher degree of symmetry is present, the analysis remains tractable. Restricting to $f(x)$ an even or odd polynomial so that:

$$f(x) = x^\sigma \prod_{i=1}^{s}(x^2 - b_i^2) \tag{5.19}$$

with b_i all real and $\sigma = 0$ or 1, we find:

$$\delta E = \frac{|N_1|\,|N_2|}{4\pi a^2}\,\mathrm{Re}\left(\left(-5 - \sum_{i=1}^{s}\frac{8}{1 - (b_i/a)^2}\right)\left((\delta x_1)^2 + (\delta x_2)^2\right)\right). \tag{5.20}$$

The alignment of cuts is parallel or perpendicular to the real axis of the complex x-plane in the energetically preferred confining vacuum when:

$$5 + \sum_{i=1}^{s}\frac{8}{1 - (b_i/a)^2} > 0 \qquad \text{(parallel)} \tag{5.21}$$

$$5 + \sum_{i=1}^{s}\frac{8}{1 - (b_i/a)^2} < 0 \qquad \text{(perpendicular)}. \tag{5.22}$$

Note that a perpendicular alignment of the cuts requires the existence of a root of $f(x)$ such that $|b_i| > |a|$. This suggests that in addition to the Coulomb attraction due to

brane/anti-brane forces, the geometry itself exerts a "torque"on the cuts. It is tempting to speculate that one possible source of torque may be the condensation of D3-branes wrapping collapsing S^3's which are not threaded by flux.

As a final example, we consider the alignment of two branch cuts where the background geometry is determined by the relation:

$$W'(x) = g \sin \frac{\pi x}{L}. \tag{5.23}$$

This corresponds to a geometry with an infinite one-dimensional lattice of minimal size S^2's located at $x = jL$ for all $j \in \mathbb{Z}$. For configurations with N_1 D5-branes at $x = mL$ and N_2 anti-D5-branes at $x = 0$, the two loop contribution to the vacuum energy density is now:

$$\delta E = \frac{|N_1|\,|N_2|}{\pi m^2 L^2} \operatorname{Re}\left((-1 + 2(-1)^m)\left((\delta x_1)^2 + (\delta x_2)^2\right)\right). \tag{5.24}$$

Thus, for m even (resp. odd) the cuts align perpendicular (resp. parallel) to the real axis of the complex x-plane.

6. Geometry and strong CP

Upon embedding our configuration in a compact Calabi-Yau, the effective θ-angle of the brane/anti-brane system becomes a dynamical field with potential determined by the vacuum energy density of the open string system. In this section we assume that the time-scale for the fluctuations of the corresponding axion is sufficiently long compared to the time-scale associated with the decay of a glueball phase to the energetically preferred confining vacuum. The axion potential is then given by minimizing the vacuum energy density over all of the confining vacua of the theory. The roots of $W'(x)$ determine the level of strong CP violation in each strongly coupled gauge group. At one loop order the effective θ-angle of the i^{th} D5-brane is defined by the relation:

$$S_i = \Lambda_i^3 = \zeta_i \,|\Lambda_i|^3 \exp\left(i\theta_i / |N_i|\right) \tag{6.1}$$

where ζ_i denotes an $|N_i|^{\text{th}}$ root of unity. The effective θ-angles now follow from equations (2.12) and (2.13):

$$\theta_i = |N_i| \arg W^{(2)}(a_i) - \sum_{i \neq j \in B} |N_j| \arg \Delta_{ij}^2 + \sum_{k \in \overline{B}} |N_k| \arg \Delta_{ik}^2 + A \qquad (N_i > 0) \tag{6.2}$$

$$\theta_i = |N_i| \arg W^{(2)}(a_i) - \sum_{i \neq k \in \overline{B}} |N_j| \arg \Delta_{ik}^2 + \sum_{j \in B} |N_k| \arg \Delta_{ij}^2 - A \qquad (N_i < 0) \tag{6.3}$$

where in the above we have absorbed all Λ_0 dependence into the single variable A:

$$A \equiv \sum_i N_i \arg \Lambda_0^2 + \theta_{\text{YM}}(\Lambda_0). \tag{6.4}$$

Note that upon rephasing the parameters $W^{(2)}(a_i)$ and Δ_{ij}^2, the value of θ_i also shifts. This is consistent with the presence of the axial anomaly. The discrete symmetry CP is preserved by the i^{th} strongly coupled gauge group when θ_i vanishes.

JHEP04(2008)052

Minimizing the vacuum energy density over all of the confining vacua yields the axion potential for the effective θ-angles:

$$V_{\rm ax} = E^{(0)} + \min\left(\delta E\right) \tag{6.5}$$

where the min denotes minimization over all of the discrete glueball phases and as before, δE denotes the second term of equation (5.1). From the perspective of the closed string dual, it is natural to view $V_{\rm ax}$ as a function of n independent variables $\theta_1, \ldots, \theta_n$. On the other hand, from the perspective of the open string description, there is a single S^2. It is therefore also natural to treat the parameter A defined in equation (6.4) as the only dynamical axion of the theory. In subsections 6.1 and 6.2 we determine constraints on the minima of $V_{\rm ax}$ by further studying the behavior of δE as a function of the θ_i's as well as the a_i's.

6.1 CP invariant submanifolds

Viewing the locations of the minimal size S^2's as an n-component vector $\overrightarrow{a} = (a_1, \ldots, a_n) \in \mathbb{C}^n$, we now argue that when l of the S^2's are occupied by a collection of branes and anti-branes and $n - l$ is sufficiently large, there exists a real submanifold of points in $\mathbb{C}^n$ with real codimension l such that the corresponding axion potential achieves a minimum at $\theta_i = 0$ for all i. It follows from equation (5.1) and the explicit expressions of appendix A that the two loop contribution to the vacuum energy density from terms linear in S_i is schematically of the form:

$$\delta E = \sum_{i \text{ occupied}} {\rm Re}\left[C_i(\overrightarrow{a}, \overrightarrow{N}) S_i\right] \tag{6.6}$$

where the $C_i(\overrightarrow{a}, \overrightarrow{N})$ are rational functions of the a_i. δE has a minimum at $\theta_i = 0$ when $C_i < 0$. The requirement that all branes and anti-branes preserve strong CP imposes l real conditions on the parameter space of the a_i's which will generically be satisfied provided $n - l$ is sufficiently large. Hence, there is a manifold of points of real dimension $2n - l$ contained in $\mathbb{C}^n$ such that all branes preserve strong CP. Note in particular that this result is independent of whether we treat all of the θ_i's or simply A as dynamical fields.

6.2 Discrete symmetries and strong CP

We now show that discrete symmetries of the Calabi-Yau translate into constraints on the amount of strong CP violation. Letting σ denote the action of the permutation symmetry on the labelling of the branes, we consider brane configurations with $W'(x)$ a polynomial with real coefficients such that $a_i = \overline{a_j} \equiv a_{\sigma(i)}$ implies $N_i = N_j$. Returning to equation (5.1) and the explicit expression for $\delta\tau$ given in appendix A, the coefficients multiplying S_i are complex conjugates of the coefficients in the analogous contribution from $S_{\sigma(i)}$. To establish this, we consider without loss of generality the θ-angle for $N_i > 0$ D5-branes at $x = a_i$.

JHEP04(2008)052

Note that:

$$Q_i \equiv \sum_{j\in\overline{B}} |N_i|\,|N_j|\,\frac{1}{W^{(2)}(a_i)}\frac{2}{\Delta_{ij}^2}\left(-1-\Delta_{ij}\frac{W^{(3)}(a_i)}{W^{(2)}(a_i)}+2\frac{W^{(2)}(a_i)}{W^{(2)}(a_j)}\right)=\overline{Q_{\sigma(i)}} \tag{6.7}$$

$$P_i \equiv \sum_{i\neq s\in B,t\in\overline{B}} |N_s|\,|N_t|\left(\frac{4}{W^{(2)}(a_s)}\frac{1}{\Delta_{si}}\frac{1}{\Delta_{st}}+(t\leftrightarrow s)+(i\leftrightarrow s)\right)=\overline{P_{\sigma(i)}}. \tag{6.8}$$

The net contribution from terms linear in S_i and $S_{\sigma(i)}$ is therefore:

$$\delta E(\theta_i) = \mathrm{Re}\,(C_i S_i) \tag{6.9}$$

$$\delta E\left(\theta_{\sigma(i)}\right) = \mathrm{Re}\left(\overline{C_i} S_{\sigma(i)}\right) \tag{6.10}$$

with C_i a complex number.

We now study the minima of the axion potential first in the case where the θ_i's are all dynamical fields, and then in the case where only A is a dynamical field. It follows from equations (6.9) and (6.10) that in the first case the minimum energy configuration satisfies $\langle\theta_i\rangle = -\left\langle\theta_{\sigma(i)}\right\rangle$. In particular, when a_i is purely real, the effective θ-angle vanishes. Next treat $V_{\rm ax}$ as a function of the single field A. In this case, the symmetries of the system in tandem with equation (6.2) yield the constraint:

$$\theta_i - A = A - \theta_{\sigma(i)} \tag{6.11}$$

so that $A = \theta_i$ when a_i is purely real. The combined contribution to the energy density from θ_i and $\theta_{\sigma(i)}$ now follows from equations (6.9) and (6.10):

$$\delta E(\theta_i)+\delta E\left(\theta_{\sigma(i)}\right) = |C_i|\,|S_i|\left(\cos\left(\gamma_i+\frac{A+2\pi k_i}{|N_i|}\right)+\cos\left(-\gamma_i+\frac{A+2\pi k_{\sigma(i)}}{|N_i|}\right)\right) \tag{6.12}$$

where in the above,

$$\gamma_i = \arg C_i + \arg S_i - \frac{A}{|N_i|}. \tag{6.13}$$

Minimizing with respect to k_i and $k_{\sigma(i)}$, the corresponding axion potential has a minimum at $A = 0$.

7. Critical points and unoccupied S^2's

To further study the phase structure of brane/anti-brane configurations wrapping S^2's in the presence of additional minimal size S^2's, we first determine the behavior of the critical points of the corresponding effective potential. As shown in [8], although it is difficult to directly solve for the critical points of the n-cut effective potential $V_{\rm eff}$, it is mathematically simpler to solve for the fluxes as a function of the critical points of $V_{\rm eff}$. In [8] these "attractor-like equations" were used to establish the gross features of multi-cut geometries. It follows from section 4 that the two cut attractor-like equations extend to geometries where only two minimal size S^2's are wrapped by branes and anti-branes. We now review the two cut attractor-like equations and then apply them in a special class of geometries

JHEP04(2008)052

and flux configurations where the analysis of the critical points remains tractable. These results are then used in section 8 to show that the breakdown in metastability is similar to the two cut geometries studied in [8].

The critical points of the two cut system satisfy two two-component vector relations [8]:

$$\frac{2i}{C}\begin{bmatrix} N_1 \\ N_2 \end{bmatrix} = \begin{bmatrix} \rho_w & 1 \\ \overline{\rho_v}\rho_w & \overline{\rho_v} \end{bmatrix} \tau \begin{bmatrix} 1 \\ -1 \end{bmatrix} - \begin{bmatrix} \rho_w & \overline{\rho_v}\rho_w \\ 1 & \overline{\rho_v} \end{bmatrix} \overline{\tau} \begin{bmatrix} 1 \\ -1 \end{bmatrix} \tag{7.1}$$

$$\frac{2i}{C}\begin{bmatrix} \alpha \\ \alpha \end{bmatrix} = \tau \begin{bmatrix} \rho_w & \overline{\rho_v}\rho_w \\ 1 & \overline{\rho_v} \end{bmatrix} \overline{\tau} \begin{bmatrix} 1 \\ -1 \end{bmatrix} - \overline{\tau} \begin{bmatrix} \rho_w & 1 \\ \overline{\rho_v}\rho_w & \overline{\rho_v} \end{bmatrix} \tau \begin{bmatrix} 1 \\ -1 \end{bmatrix} \tag{7.2}$$

where τ is the 2×2 period matrix, C is a constant non-zero complex number, and we have introduced:

$$\rho_v = -\frac{d_3 \pm \sqrt{d_3^2 - 4d_1d_2}}{2d_2} \tag{7.3}$$

$$\rho_w = -\frac{d_3 \pm \sqrt{d_3^2 - 4d_1d_2}}{2d_1} \tag{7.4}$$

with:

$$d_1 = \det \begin{bmatrix} \mathcal{F}_{111} & \mathcal{F}_{112} \\ \mathcal{F}_{112} & \mathcal{F}_{122} \end{bmatrix}, \; d_2 = \det \begin{bmatrix} \mathcal{F}_{112} & \mathcal{F}_{122} \\ \mathcal{F}_{122} & \mathcal{F}_{222} \end{bmatrix}, \; d_3 = \det \begin{bmatrix} \mathcal{F}_{111} & \mathcal{F}_{112} \\ \mathcal{F}_{122} & \mathcal{F}_{222} \end{bmatrix}. \tag{7.5}$$

The $\pm$ signs of equations (7.3) and (7.4) are correlated. The requirement that $g_{\rm YM}^2 > 0$ leads to an unambiguous assignment of brane type for each branch. Switching from the $+$ to the $-$ branch of equations (7.3) and (7.4) changes all branes (anti-branes) into anti-branes (branes).

Next consider more general geometries with:

$$W'(x) = g(x^2 - a^2)f(x) \tag{7.6}$$

where $g, a > 0$ and $f(x)$ is an even or odd polynomial whose roots are all isolated and real. This corresponds to a geometry where the minimal size S^2's are situated along the real axis of the complex x-plane and are symmetrically arranged with respect to the imaginary axis. We take $N_1 > 0$ branes at $x = a_1 = a$ and $N_2 < 0$ anti-branes at $x = a_2 = -a$ with the remaining minimal size S^2's left unwrapped by branes.

We now show that when $N_1 = -N_2$, the corresponding effective potential admits critical points such that $t_1 = \overline{t_2}$. The analysis is very similar to that given in [8] and we will therefore only summarize the various steps in the computation. It follows from the $\mathbb{Z}_2$ symmetry of the configuration that there exists a finite neighborhood around $t_1, t_2 = 0$ such that for $t_1 = \overline{t_2}$ we have:

$$\begin{bmatrix} \overline{\tau_{11}} & \overline{\tau_{12}} \\ \overline{\tau_{12}} & \overline{\tau_{22}} \end{bmatrix} = \begin{bmatrix} -\tau_{22} & -\tau_{12} \\ -\tau_{12} & -\tau_{11} \end{bmatrix} - \frac{M - \overline{M}}{2\pi i} \begin{bmatrix} 1 & 1 \\ 1 & 1 \end{bmatrix} \tag{7.7}$$

$$\mathcal{F}_{111} = (-1)^{\deg f}\overline{\mathcal{F}_{222}} \tag{7.8}$$

$$\mathcal{F}_{112} = (-1)^{\deg f}\overline{\mathcal{F}_{122}} \tag{7.9}$$

where $M \equiv \log\left(\Lambda_0^2/\Delta^2\right)$. This implies $d_1 = \overline{d_2}$, $d_3 = \overline{d_3}$ and thus, $\overline{\rho_v} = \rho_w$. Returning to equations (7.1) and (7.2), $t_1 = \overline{t_2}$ implies $N_1 = -N_2$ and:

$$\frac{\alpha}{N_1} = \frac{1+\rho_w}{1-\rho_w}\left(\tau_{11} + \tau_{12} + \frac{M-\overline{M}}{2\pi i}\right) + \frac{\tau_{22}-\tau_{11}}{1-\rho_w}. \tag{7.10}$$

8. Breakdown of metastability revisited

In two cut geometries with $N_1 = -N_2$ and both branch cuts aligned along the real axis of the complex x-plane, there is a critical amount of flux beyond which the effective potential ceases to admit critical points for t_i small [8]. Viewing the ratio α/N_1 as a function of the real modulus $t \equiv t_1 = t_2 > 0$, a critical point of this function corresponds to the merging of a local minimum and maximum of V_{eff}. In this section we study the analogous situation when additional minimal size S^2's are present in the open string description of the system.

Based on the condition for a breakdown in metastability in two cut geometries given by equation (2.16), our expectation is that two loop effects will destabilize the metastable vacua when the one loop vacuum energy density becomes comparable to the energy density of a supersymmetric brane configuration. Testing this expectation requires determining the attractor-like equations for more general flux configurations and then determining when the effective potential experiences a merger of two critical points. Although for general configurations this appears to be intractable with present techniques, when the branes and anti-branes of the open string description cluster into two groups so that the system is characterized by the brane/anti-brane distance Δ_{sep} and the internal separation scale within a cluster Δ_{inter} with $|\Delta_{\text{inter}}| \ll |\Delta_{\text{sep}}|$, the analysis reduces to that of the two cut system. Indeed, it follows from general renormalization group arguments that at energy scales above the mass scale set by Δ_{inter}, each cluster of branes will behave as a single stack of "unHiggsed"branes. In this case the expected breakdown in metastability is given by the general bound for the two cut system:

$$\frac{8\pi}{g_{\text{YM}}^2}\left(|N_1| + |N_2|\right) - \frac{2}{\pi}|N_1|\,|N_2| \log\left|\frac{\Lambda_0}{\Delta_{\text{sep}}}\right|^2 \gtrsim \frac{8\pi}{g_{\text{YM}}^2}|N_1 + N_2| \tag{8.1}$$

where $N_1 > 0$ denotes the net number of branes from the first cluster and $N_2 < 0$ denotes the net number of anti-branes from the second cluster. This is indeed consistent with expectations based on treating the branes in the geometry as a distribution of point charges. For more general configurations the precise bound on the one loop contribution is more involved because the channel of brane/anti-brane annihilation depends on the relative positions of all branes and anti-branes in the geometry. This complicates the estimate of when to expect a breakdown in metastability.

To avoid such subtleties, in the rest of this section we restrict our analysis to configurations with $N_1 = N > 0$ D5-branes at $x = a_1 = a > 0$ and $N_2 = -N$ anti-D5-branes at $x = a_2 = -a$ in geometries with:

$$W'(x) = g(x^2 - a^2)f(x) \tag{8.2}$$

and $f(x)$ as in equation (5.19). It follows from the results of section 7 that in this case there exist critical points which satisfy $t_1 = \overline{t_2} \equiv t$. Using the explicit expressions for τ_{ij} and $\mathcal{F}_{ijk}$ given in appendix B, expanding equation (7.10) to lowest order in $r > 0$ with $t = e^{i\phi}r$ yields:

$$\frac{2\pi i\alpha}{N} = \pm\left(1 + 2(-1)^{\deg f} e^{\pm i\phi}\beta r\right)\left(\log\left(re^{i\phi}\right) - \log\left|\frac{\Lambda_0}{\Delta}\right|^4\right) + \mathcal{O}(r) + \mathcal{O}(r^2\log r) \quad (8.3)$$

where the variable β is defined by equation (B.11) in appendix B. Because the results of subsection 5.2 establish that the minimal energy confining vacuum corresponds to a configuration where the branch cuts align parallel or perpendicular to the real axis of the complex x-plane, it is enough to study the critical points of $2\pi i\alpha/N$ as a function of $t \in \mathbb{R}$. Further, due to the fact that each value of $\theta_{\rm YM}$ will be attained by some value of r by changing ϕ by a small amount, it is enough to demonstrate that $\mathrm{Re}[2\pi i\alpha/N]$ has an extremum as a function of r for $\phi = 0$ or π.

At leading order in r, the critical points of $\mathrm{Re}\,[2\pi i\alpha/N]$ satisfy:

$$\frac{1}{r_*} = -2(-1)^{\vartheta+\deg f}\beta\log\left(r_*\left|\frac{\Delta}{\Lambda_0}\right|^4\right) \quad (8.4)$$

where the variable $\vartheta = 0$ for $\phi = 0$ and $\vartheta = 1$ for $\phi = \pi$. The existence of a critical point therefore requires $(-1)^{\vartheta+\deg f}\beta > 0$. Returning to the definition of β given by equation (B.11) in appendix B, note that this inequality is in accord with the condition for parallel ($\vartheta = 0$) and perpendicular ($\vartheta = 1$) alignment given by equations (5.21) and (5.22), respectively.

The critical value of the 't Hooft coupling $\lambda = g_{\rm YM}^2 N$ for which the system is no longer metastable is given by evaluating equation (8.3) at the value determined by equation (8.4). Dropping all subleading logarithms, a crude estimate of this value is:

$$\frac{8\pi^2}{\lambda_*} = \log\left|\frac{\Lambda_0}{\Delta}\right|^4 + \log\left|20 + \sum_{i=1}^{s}\frac{32}{1-(b_i/a)^2}\right|. \quad (8.5)$$

8.1 Endpoints and further transitions

As shown in [8] for the two cut system, once metastability is lost, the sizes of the cuts will expand in order to facilitate the annihilation of flux lines. This expansion leads to the collapse of a 3-cycle in the geometry, at which point additional light degrees of freedom enter the low energy spectrum. Whereas the presence of D5-branes wrapping this collapsed 3-cycle tend to relax the system back to a metastable geometry of lower flux, the presence of a D3-brane wrapping this 3-cycle can drive the system to a non-Kähler geometry.

Even though the alignment of cuts for metastable vacua is sometimes perpendicular and sometimes parallel to the real axis of the complex x-plane, in all cases that we have studied numerically the mode of instability drives the cuts to align and expand along the real axis of the complex x-plane once metastability is lost.

As opposed to the two cut geometry, however, for more general flux configurations a branch cut supported by flux may first collide with another cut supported by flux of the

JHEP04(2008)052

same sign. In this case, the presence of D5-branes wrapping the collapsing 3-cycle separate vacua in the four dimensional spacetime which are nearly degenerate in energy density. Hence, in comparison to the two cut geometry, a D3-brane wrapping this same collapsed cycle will play a more pronounced rôle in determining the endpoint of this transition. Note, however, that generic values of $\theta_{\rm YM}$ can also prevent such collisions. Indeed, whereas $\theta_{\rm YM}$ tends to tip branch cuts supported by positive and negative RR fluxes so that they will continue to collide, when both branch cuts support flux of the same sign, they tip so as to remain parallel.

9. Modes of annihilation

When $W'(x)$ has two roots, the branes and anti-branes eventually annihilate by traversing an interpolating minimal size 3-chain. In this section we demonstrate that for more general geometries, new modes of brane/anti-brane annihilation appear or disappear as the locations of the minimal size S^2's change.

This is mathematically similar to the problem of determining the BPS spectrum of $\mathcal{N} = 2$ gauge theories geometrically engineered in type IIB string theory on geometries of the form:

$$y^2 = P(x) + uv \tag{9.1}$$

where $P(x)$ is a polynomial with isolated roots. The spectrum of solitons given by D3-branes wrapping supersymmetric 3-cycles which interpolate between the roots of $P(x)$ depends strongly on the relative positions of these roots [37]. As a particular example, when the roots of $P(x)$ are all located on the real axis of the complex x-plane and ordered as $r_n < \ldots < r_1$, the BPS soliton connecting r_n to r_1 decays into a collection of $n-1$ BPS solitons joining r_i to r_{i-1} for $1 < i < n+1$ [37].

We are interested in a special limit of the above analysis where $P(x) \simeq W'(x)^2$. In this case the BPS spectrum will be similar to that determined by two dimensional $\mathcal{N} = (2,2)$ Landau-Ginzburg theory [37]. It follows from arguments similar to those presented in [37] that the spectrum of nearly BPS D5-branes wrapping 3-cycles will develop instabilities as the roots of $W'(x)$ change.

In the next two subsections we restrict our analysis for illustrative purposes to geometries with three minimal size S^2's. We determine the wall of marginal stability for a D5-brane domain wall solution wrapping a 3-chain connecting two roots of $W'(x)$ to decay to a two domain wall process. We next demonstrate that such solutions have minimal tension. This implies that for more general geometries, semi-classical brane/anti-brane annihilation proceeds via a multi-stage "hopping"process. Finally, in subsection 9.3 we indicate some qualitative features of this phenomenon.

9.1 Spectrum of nearly BPS domain walls with three minimal S^2's

We now determine the nearly BPS spectrum of D5-branes wrapping interpolating 3-chains in geometries with three minimal size S^2's. Given a 3-chain interpolating between $x = a_i$

and $x = a_j$, the tension of the corresponding domain wall is well-approximated by:

$$T\left[\gamma_{ij}\right] = \frac{1}{g_s}\int_{\gamma_{ij}} \left|W'(x)\right| |dx| \tag{9.2}$$

where γ_{ij} denotes a contour in the complex x-plane. For a single nearly BPS domain wall, the tension is:

$$T_{ij} = \frac{1}{g_s}\left|W\left(a_i\right) - W\left(a_j\right)\right| \tag{9.3}$$

corresponding to a path in the complex x-plane such that the phase of $W'(x)$ remains constant for all $x \in \gamma_{ij}$.

An important caveat to equation (9.3) is that it assumes the existence of a single nearly BPS domain wall. Letting $a_1 = -a_2 = a > 0$ and $a_3 = c$, note that $c = 0$ implies $W(a) = W(-a)$ so that the purported domain wall solution connecting a and $-a$ would have zero tension. This unphysical result establishes the absence of such a single BPS domain wall in this region of configuration space. We now determine the wall of marginal stability for a single BPS domain wall to decay into two constituent products. The central charge of each candidate BPS domain wall is:

$$Z_{ij} = W\left(a_j\right) - W\left(a_i\right). \tag{9.4}$$

The wall of marginal stability corresponds to the locus of non-trivial c values such that the phases of the central charges for the candidate decay products align. Setting $c/a \equiv R + iI$, the defining equation for the wall of marginal stability is:

$$I_{\mathrm{MS}}(R) = \pm\sqrt{R^2 - 3 + 2\sqrt{R^4 - 3R^2 + 3}}. \tag{9.5}$$

See figure 6 for the region of marginal stability in the R-I plane. Assuming that the brane/anti-brane configuration spontaneously breaks $\mathcal{N} = 2$ supersymmetry, the overall shape of this wall of marginal stability should remain correct up to $1/N$ corrections.

9.2 Tension minimizing solutions

When a single nearly BPS domain wall solution ceases to exist, the total tension of the resulting decay products is a global minimum of the tension formula given by equation (9.2). To establish this, let $x(t)$ denote a parametrization of the path γ_{12} which runs from $x(0) = a_1$ to $x(1) = a_2$. It follows from the Cauchy-Riemann equations that the net tension of the D5-brane wrapping the corresponding 3-chain is:

$$T\left[\gamma_{12}\right] = \frac{1}{g_s}\int_0^1 \left|\left(\dot{W}_1\right)^2 + \left(\dot{W}_2\right)^2\right|^{1/2} dt \tag{9.6}$$

where we have decomposed W into real and imaginary parts so that $W = W_1 + iW_2$. Equation (9.6) implies that minimum tension paths in the complex x-plane map to piecewise straight line paths in the complex W-plane.

JHEP04(2008)052

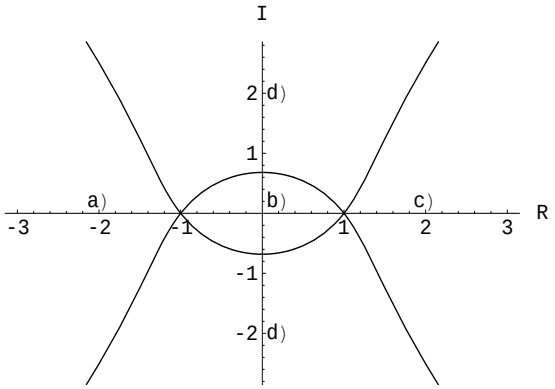

Figure 6: Plot of the walls of marginal stability with three minimal size S^2's located at $a_1 = 1$, $a_2 = -1$ and $a_3 = R + iI$. As the point a_3 is varied throughout the $R - I$ plane, a single BPS domain wall solution connecting two of the a_i's may decay into a two stage process. When a_3 is located in region a), the process $a_3 \to a_1$ decays. For a_3 in region b), the process $a_2 \to a_1$ decays and in region c) the process $a_2 \to a_3$ decays. In region d) all processes of the form $a_i \to a_j$ are allowed.

To demonstrate that the two product process described in the previous subsection minimizes T, we first restrict to the case with $a_3 = iL$ and $L \in \mathbb{R}$. In the complex W-plane the decay products of the domain wall solution connecting a to $-a$ map to a straight line connecting $W(a)$ to $W(iL)$ and a further straight line connecting $W(iL)$ to $W(-a)$. The values of $W(\pm a)$ and $W(iL)$ in the complex W-plane are:

$$W(\pm a) = \frac{g}{12} a^4 \left(-3 \pm 8i \frac{L}{a} \right) \tag{9.7}$$

$$W(iL) = \frac{g}{12} L^4 \left(-1 - 6 \frac{a^2}{L^2} \right) \tag{9.8}$$

so that for $g > 0$, the locations of $W(\pm a)$ correspond to reflections across the real axis of the complex W-plane. On the other hand, for $-|I_{\rm MS}(R=0)| < L < |I_{\rm MS}(R=0)|$, $\mathrm{Re}\,[W(iL)] > \mathrm{Re}\,[W(\pm a)]$ so that $W(iL)$ lies to the right of $W(\pm a)$ in the complex W-plane. While the shortest path between the points $W(a)$ and $W(-a)$ in the complex W-plane corresponds to a straight vertical line, this may not correspond to a path in the complex x-plane. Indeed, consider any path in the complex x-plane connecting $x = a$ to $x = -a$. Such a path will necessarily attain the value $x = iy$ for some $y \in \mathbb{R}$. In the complex W-plane, the path must therefore pass through the value $W(iy)$. Comparing the values of $W(iy)$ and $W(iL)$, we find:

$$W(iy) - W(iL) = \frac{g}{12} (L - y)^2 \left(6a^2 + 2y^2 + (L + y)^2 \right) > 0. \tag{9.9}$$

Hence, when $\mathrm{Re}\,[W(iL)] > \mathrm{Re}\,[W(\pm a)]$, the piecewise straight line path in the complex W-plane will be shortest when $y = L$. Performing an arbitrary real deformation of a_3 away from the imaginary axis, it now follows that for all points which lie within the region bounded by the marginal stability curves given by equation (9.5), the decay products of the single nearly BPS domain wall solution minimize the tension functional of equation (9.2).

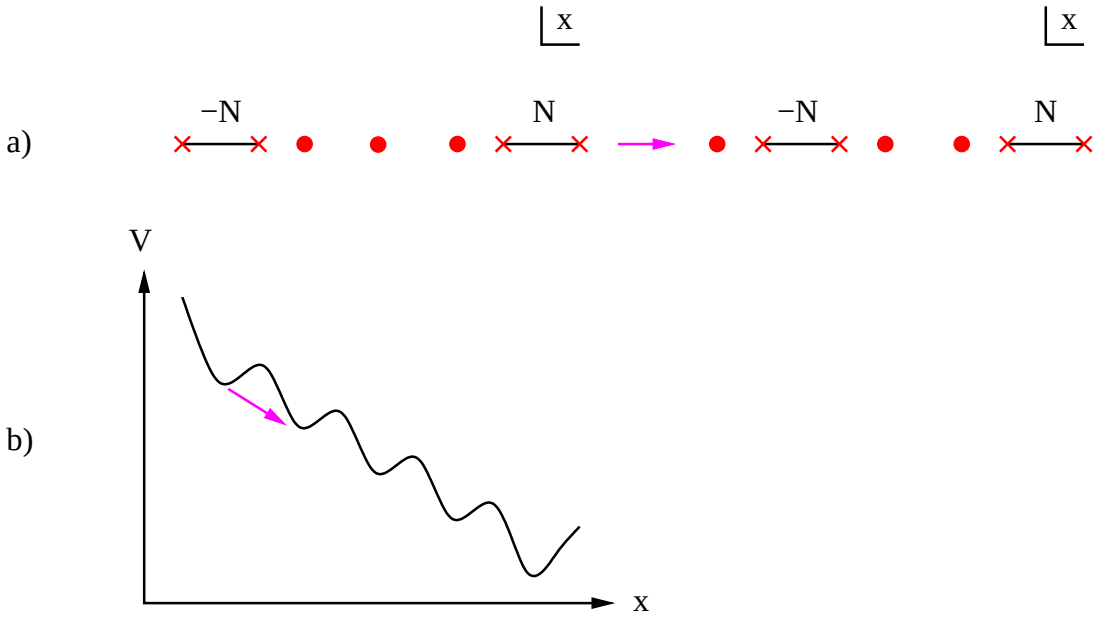

Figure 7: The positions of the roots of $W'(x)$ can sometimes obstruct flux line annihilation in the closed string dual geometry. Instead, the flux must perform discrete jumps to other cuts before annihilating. In (a) a hopping event where all $-N$ units of flux transfer to another cut is shown. The effective potential as a function of $x \in \mathbb{R}$ seen by the branes is shown in (b).

9.3 Hopping effects

Upon wrapping branes and anti-branes on two minimal size S^2's, the results of the previous subsection show that the additional S^2's present in the geometry can sometimes obstruct direct brane/anti-brane annihilation. In a semi-classical n-domain wall decay process, a collection of branes tunnels from one minimal size S^2 to the next until finally annihilating with an anti-brane at the n^{th} stage. In the closed string dual description, flux lines hop from cut to cut before annihilating. The system lowers its energy during each intermediate stage due to the one loop contribution to the vacuum energy density from terms proportional to $\log|a_{\text{brane}} - a_{\text{anti-brane}}|$. Because the tensions of the domain wall solutions are all comparable, the rate of decay due to hopping is much slower than direct annihilation. See figure 7 for a depiction of this phenomenon. In this subsection we discuss some further consequences which follow from hopping effects.

Letting $\Gamma_{i\to i+1}$ denote the decay rate per unit volume for branes to tunnel from $x = a_i$ to $x = a_{i+1}$, the rate for an n-stage annihilation event which begins with $i = 1$ and ends with $i = n + 1$ is given by summing over the inverse rates of each individual link in the decay chain:[1]

$$\Gamma_{\text{net}}^{-1} = \sum_{i=1}^{n} \Gamma_{i\to i+1}^{-1} \tag{9.10}$$

[1] In this formula we assume that each successive bubble of vacuum can nucleate anywhere within the four dimensional Minkowski spacetime. This provides an adequate approximation of the decay of the false vacuum because the decay rate of each term in the decay chain is exponentially suppressed.

JHEP04(2008)052

so that a single hopping event can significantly retard the time-scale for a drop in the total number of branes in the system.

Recall that in the dual closed string description there is a critical amount of flux which can thread an S^3 before metastability is lost. It follows that in certain cases a hopping event can trigger a breakdown in metastability when too much flux threads an S^3. Combining this with the discussion in subsection 8.1, this provides a completely dynamical mechanism whereby a system can begin in a metastable Calabi-Yau geometry and transition to a non-Kähler geometry.

As a collection of branes hops from one site to the next, the energetically preferred direction of alignment for the branch cuts can also change. As a simple example, consider the alignment of branch cuts in the geometry given by an infinite one-dimensional lattice of evenly spaced minimal size S^2's of the type studied in subsection 5.2. For a pair of branes and anti-branes separated by m lattice sites, the associated branch cuts align parallel to the real axis for m odd, and perpendicular to the real axis for m even. As the branes begin to hop towards one another, the energetically preferred orientation of the cuts will also change.

The minima of the axion potential determined by equation (5.1) will also change. Indeed, if the number of occupied minimal size S^2's changes from l to l', it follows from the analysis of subsection 6.1 that when $n-l$ and $n-l'$ are both sufficiently large, the manifold of points $(a_1,\ldots,a_n)\in\mathbb{C}^n$ which preserve strong CP will change from real dimension $2n-l$ to $2n-l'$.

10. Radial mode stabilization and glueball phases

In this section we propose a speculative mechanism which may stabilize the radial mode in *compact* Calabi-Yau threefolds. Interpreting the two loop contribution to the vacuum energy density as a radial potential, we now show that when the phases of the glueball fields anti-align with the energetically preferred confining vacuum, this potential contains a power law repulsion term which can counter the Coulomb attraction term present at one loop.

For simplicity we first consider a two cut configuration with $N_1=N$ D5-branes and $N_2=-N$ anti-D5-branes separated by a distance $\Delta=a_1-a_2$. Treating $\theta_{\rm YM}$ as a mode which has already developed an expectation value, we identify the two loop corrected value of the vacuum energy density with the radial potential:

$$V_{\rm rad}(\Delta)=\frac{16\pi N}{g_{\rm YM}^2}-\frac{2N^2}{\pi}\log\left|\frac{\Lambda_0}{\Delta}\right|^2 \tag{10.1}$$

$$-\frac{20N^2}{\pi}\left|\frac{\Lambda_0}{\Delta}\right|^4 e^{-8\pi^2/\lambda}\left(\cos\frac{2\pi k+\theta_{\rm YM}}{N}+\cos\frac{2\pi l+\theta_{\rm YM}}{N}\right) \tag{10.2}$$

where we have introduced the 't Hooft coupling $\lambda=g_{\rm YM}^2N$ and k and l are integers which label the distinct confining vacua of the system. Note that whereas the second term produces a logarithmic attraction between the branes and anti-branes, the sign of the power law contribution to $V_{\rm rad}(\Delta)$ crucially depends on the particular confining vacuum of the system. Assuming that the time-scale for the fluctuations of the radial mode are sufficiently

JHEP04(2008)052

fast in comparison to the time-scale[2] for the decay of the glueball phase to the energetically preferred alignment configuration, it follows that there exists a stable minimum of $V_{\rm rad}(\Delta)$ for $k, l \sim N/2$ given by:

$$|\Delta_*|^4 = -20\,|\Lambda_0|^4\, e^{-8\pi^2/\lambda}\left(\cos\frac{2\pi k+\theta_{\rm YM}}{N}+\cos\frac{2\pi l+\theta_{\rm YM}}{N}\right). \tag{10.3}$$

Although highly suggestive, it is unclear whether this mechanism is consistent with the stabilization of the other moduli of the system. Indeed, it follows from the analysis of [8] as well as section 8 that in the two cut geometry the size of the glueball fields becomes unstable when equation (8.4) holds so that:

$$\log\left|\frac{\Lambda_0}{\Delta}\right|^4 \sim \frac{1}{20t_*} = \frac{1}{20}\left|\frac{\Delta}{\Lambda_0}\right|^4 e^{8\pi^2/\lambda} \tag{10.4}$$

where in the last equality we have approximated t_* by its one loop value. This expression is of the same order of magnitude as equation (10.3). Assuming $k, l \sim N/2$, simultaneously satisfying equation (10.3) and the condition $t < t_*$ requires:

$$0 < \log\left|\frac{\Lambda_0}{\Delta}\right|^4 < 2 \tag{10.5}$$

which is not consistent with an expansion in large Λ_0. Thus, at the level of analysis presented here, we cannot definitively conclude one way or the other whether misaligned glueball phases will stabilize the radial mode.

Adding additional S^2's does not naïvely resolve the difficulties encountered above. For simplicity, we neglect fluctuations corresponding to the motion of unoccupied minimal size S^2's and consider symmetric configurations of minimal size S^2's of the type considered in section 8. It follows from equation (8.4) that the size of the glueball field develops an instability at a value comparable to that given by equation (10.4) where the factor of 20 is now replaced by $|2\beta|$, with β as in equation (B.11) of appendix B. On the other hand, this same replacement will also occur in equation (10.3).

Before concluding this section, we note that strictly speaking, the analysis of section 6 assumes the existence of another mechanism to stabilize the radial mode. This is because the axion potential was obtained by minimizing over all glueball phases.

11. Conclusions and discussion

Changing the location of minimal size S^2's triggers phase transitions in geometrically metastable configurations given by branes and anti-branes wrapping homologous minimal size S^2's in a non-compact Calabi-Yau threefold. While two loop effects appear to

[2]Whereas in the axion potential discussion we took the scale of fluctuations for $\theta_{\rm YM}$ to be sufficiently large compared to all such glueball phase alignment decay events, here we assume that the radial mode fluctuates more rapidly. As computed in [8], when the size of the glueball field is not exponentially suppressed this decay rate is an exponentially suppressed quantity so that there are typically a wide range of energy scales available at which individual modes become relevant for the analysis.

JHEP04(2008)052

generically lift the degeneracy in vacua present in supersymmetric confining vacua, changing the relative positions of the S^2's causes discrete jumps in which confining vacuum has minimal energy density. The minima of the associated axion potential are also constrained by the discrete symmetries of a given configuration. Although the presence of additional S^2's does not alter the qualitative conditions for a breakdown in metastability, their presence leads to the existence of walls of marginal stability for nearly BPS brane/anti-brane annihilation processes. This generates novel phase dynamics where branes "hop" to nearby minimal size S^2's. Although far from conclusive, when the glueball phases anti-align with the energetically preferred vacuum, the two loop correction to the vacuum energy density may stabilize the radial mode present in any compact Calabi-Yau threefold geometry. In the rest of this section we discuss some implications of this work and some possible avenues of future investigation.

Over suitable time-scales, the ranks of the low energy gauge groups will dynamically redistribute due to hopping effects. This leads to a statistical distribution of gauge groups connected by such events. It is intriguing that for geometries with a large number of minimal size S^2's, hopping would seem to favor gauge groups with a large number of low rank gauge group factors.

Along similar lines, the statistical mechanics of hopping may also be of independent interest. In geometries with a large grid of unoccupied minimal size S^2's, one can arrange for a "current" of branes to flow along the grid. It is natural to speculate on the existence of suitable conditions leading to superconductivity in this setup. In the case of a one dimensional lattice of minimal size S^2's, the presence of hopping also suggests connections with the physics of spin chains, with the unoccupied S^2's playing the role of impurities. It would be interesting to see whether statistical correlations in such systems undergo phase transitions as one increases the "doping" of the system.

It may also be important to determine the consequences of hopping from the perspective of a four dimensional observer. As one possibility, note that in some cases a multi-stage bubble nucleation process will lead to a collision between distinct bubbles. While the collision of such bubbles of vacuum has been studied from various perspectives, it would be interesting to see how the results of this paper fit with these other developments.

Walls of marginal stability for brane/anti-brane annihilation processes are most likely a generic feature of compact Calabi-Yau threefolds, although there are likely to be further features specific to the compact case. For example, the corresponding domain wall solutions may not factorize as the product of a path on a local Riemann surface with an S^2 fibration. Determining the "mean free path" for such obstructions in a compact Calabi-Yau threefold would be interesting.

There are many additional subtleties present for brane/anti-brane systems on compact Calabi-Yau threefolds. In addition to α' corrections to the form of the Kähler metric, one must also find a mechanism which stabilizes all of the non-normalizable modes of the non-compact case. It is very suggestive that glueball fields with phases anti-aligned with the energetically preferred confining vacuum generate a power law repulsion term which can naïvely stabilize the radial mode of a brane/anti-brane system. Because this result is highly contingent on the phase of the glueball fields, in the absence of another mechanism,

JHEP04(2008)052

stabilization of the radial mode would appear to preferentially select metastable confining vacua with *maximal* rather than minimal energy density. Note that this is somewhat at odds with the procedure outlined in section 6 for extracting the axion potential by minimizing over all glueball phases. It is likely that further phase structure results from the interplay between the stabilization of the axion, the radial mode, and the other closed string modes of compact Calabi-Yau threefolds.

Acknowledgments

We thank J. Seo for many helpful discussions and collaboration at an early stage of this work. In addition, we thank M. Aganagic, C. Beasley, M.R. Douglas, A.L. Fitzpatrick, S. Kachru, J. Marsano, K. Papadodimas, M. Shigemori and L.-S. Tseng for helpful discussions. CV thanks the CTP at MIT for hospitality during his sabbatical leave, where part of this work was completed. The work of the authors is supported in part by NSF grants PHY-0244821 and DMS-0244464. The research of JJH is also supported by an NSF Graduate Fellowship.

A. Two loop corrections to τ_{ij}

In this appendix we collect the two loop corrections to τ_{ij} derived in section 3. For $i \neq j$ we have:

$$2\pi i\tau_{ij} = -\log\frac{\Lambda_0^2}{\Delta_{ij}^2} + \frac{1}{W^{(2)}(a_i)}\frac{2}{\Delta_{ij}^2}\left(-1-\Delta_{ij}\frac{W^{(3)}(a_i)}{W^{(2)}(a_i)}+2\frac{W^{(2)}(a_i)}{W^{(2)}(a_j)}\right)S_i \tag{A.1}$$

$$+\frac{1}{W^{(2)}(a_j)}\frac{2}{\Delta_{ji}^2}\left(-1-\Delta_{ji}\frac{W^{(3)}(a_j)}{W^{(2)}(a_j)}+2\frac{W^{(2)}(a_j)}{W^{(2)}(a_i)}\right)S_j \tag{A.2}$$

$$+\sum_{k\notin\{i,j\}}\left(\frac{4}{W^{(2)}(a_i)\Delta_{ij}\Delta_{ik}}+\frac{4}{W^{(2)}(a_j)\Delta_{ji}\Delta_{jk}}+\frac{4}{W^{(2)}(a_k)\Delta_{ki}\Delta_{kj}}\right)S_k+\mathcal{O}(S^2) \tag{A.3}$$

and, for terms on the diagonal:

$$2\pi i\tau_{ii} = \log\frac{S_i}{W^{(2)}(a_i)\Lambda_0^2}+\left(\frac{W^{(3)}(a_i)^2}{W^{(2)}(a_i)^3}-\frac{1}{2}\frac{W^{(4)}(a_i)}{W^{(2)}(a_i)^2}\right)S_i$$

$$+\sum_{i\neq j}\frac{1}{W^{(2)}(a_i)}\frac{2}{\Delta_{ij}^2}\left(-1-\Delta_{ij}\frac{W^{(3)}(a_i)}{W^{(2)}(a_i)}+2\frac{W^{(2)}(a_i)}{W^{(2)}(a_j)}\right)S_j+\mathcal{O}(S^2).$$

As a check on the above computations, we next compare our value of the two loop correction to τ which we denote by $\delta\tau$ with the known values for the two and three cut geometries. When $W'(x) = g(x-a_1)(x-a_2)$, this reduces to:

$$2\pi i\delta\tau_{11}^{2-\text{cut}} = 4\frac{S_1}{g\Delta_{12}^3}-10\frac{S_2}{g\Delta_{12}^3} \tag{A.4}$$

$$2\pi i\delta\tau_{12}^{2-\text{cut}} = -10\frac{S_1}{g\Delta_{12}^3}+10\frac{S_2}{g\Delta_{12}^3} \tag{A.5}$$

which agrees with appendix B of [39].

When $W'(x) = g(x-a_1)(x-a_2)(x-a_3)$, we find:[3]

$$2\pi i\delta\tau_{11}^{3-\text{cut}} = \frac{1}{g\Delta_{12}^2\Delta_{13}^2}\left(5+4\frac{\Delta_{13}}{\Delta_{12}}+4\frac{\Delta_{12}}{\Delta_{13}}\right)S_1 \tag{A.6}$$

$$+\frac{2}{g\Delta_{12}^2\Delta_{13}\Delta_{23}}\left(-2+5\frac{\Delta_{23}}{\Delta_{21}}-2\frac{\Delta_{32}}{\Delta_{31}}\right)S_2 \tag{A.7}$$

$$+\frac{2}{g\Delta_{13}^2\Delta_{12}\Delta_{32}}\left(-2+5\frac{\Delta_{32}}{\Delta_{31}}-2\frac{\Delta_{23}}{\Delta_{21}}\right)S_3 \tag{A.8}$$

$$2\pi i\delta\tau_{12}^{3-\text{cut}} = \frac{2}{g\Delta_{12}^2\Delta_{13}\Delta_{23}}\left(-2+5\frac{\Delta_{23}}{\Delta_{21}}-2\frac{\Delta_{32}}{\Delta_{31}}\right)S_1 \tag{A.9}$$

$$-\frac{2}{g\Delta_{21}^2\Delta_{23}^2}\left(2+2\frac{\Delta_{32}}{\Delta_{31}}+5\frac{\Delta_{23}}{\Delta_{21}}\right)S_2 \tag{A.10}$$

$$+\frac{8}{g\Delta_{12}\Delta_{13}\Delta_{23}^2}\left(1-\frac{\Delta_{23}}{\Delta_{21}}-\frac{\Delta_{32}}{\Delta_{31}}\right)S_3 \tag{A.11}$$

which agrees[4] with appendix C of [41].

B. Two cut τ_{ij} with n minimal size S^2's

In this appendix we compute the form of the period matrix when:

$$W'(x) = g(x-a_1)(x-a_2)f(x) \tag{B.1}$$

where f is a polynomial with isolated roots and all A-cycle periods other than S_1 and S_2 are formally set to zero, in accord with the discussion in section 4.

Setting $t_i \equiv S_i/(W^{(2)}(a_i)\Delta_{12}^2)$, it follows from the expressions given in appendix A that the relevant matrix entries are:

$$2\pi i\tau_{11} = \log\left(t_1\frac{\Delta_{12}^2}{\Lambda_0^2}\right)+\left[\left(2+\frac{2\Delta_{12}f'(a_1)}{f(a_1)}\right)^2-\frac{\Delta_{12}}{2}\frac{6f'(a_1)+3\Delta_{12}f^{(2)}(a_1)}{f(a_1)}\right]t_1 \tag{B.2}$$

$$+\left[4+2\frac{f(a_2)}{f(a_1)}+4\frac{f(a_2)}{f(a_1)}\left(1+\frac{\Delta_{12}f'(a_1)}{f(a_1)}\right)\right]t_2+\mathcal{O}(t^2) \tag{B.3}$$

$$2\pi i\tau_{12} = -\log\frac{\Lambda_0^2}{\Delta_{12}^2}+\left[-6-4\frac{f(a_1)}{f(a_2)}-4\frac{\Delta_{12}f'(a_1)}{f(a_1)}\right]t_1 \tag{B.4}$$

$$+\left[-6-4\frac{f(a_2)}{f(a_1)}+4\frac{\Delta_{12}f'(a_2)}{f(a_2)}\right]t_2+\mathcal{O}(t^2) \tag{B.5}$$

$$2\pi i\tau_{22} = \log\left(t_2\frac{\Delta_{12}^2}{\Lambda_0^2}\right)+\left[\left(2-\frac{2\Delta_{12}f'(a_2)}{f(a_2)}\right)^2+\frac{\Delta_{12}}{2}\frac{6f'(a_2)-3\Delta_{12}f^{(2)}(a_2)}{f(a_2)}\right]t_2 \tag{B.6}$$

$$+\left[4+2\frac{f(a_1)}{f(a_2)}+4\frac{f(a_1)}{f(a_2)}\left(1-\frac{\Delta_{12}f'(a_2)}{f(a_2)}\right)\right]t_1+\mathcal{O}(t^2). \tag{B.7}$$

[3] We thank J. Seo for suggesting this check.

[4] In appendix C of [41], the sign of what is referred to as h_{ab} should be reversed in the period Π_a. This is easily checked (and remedied) by appealing to the symmetry of the τ matrix entries under permutation of its indices.

JHEP04(2008)052

When $f(x)$ is an even or odd polynomial whose roots are all isolated and real, the entries of τ_{ij} and $\mathcal{F}_{ijk}$ simplify further:

$$\begin{bmatrix} 2\pi i\tau_{11} & 2\pi i\tau_{12} \\ 2\pi i\tau_{12} & 2\pi i\tau_{22} \end{bmatrix} = \begin{bmatrix} \log\left(t_1 \frac{\Delta_{12}^2}{\Lambda_0^2}\right) + \gamma t_1 + \beta t_2 & -\log\frac{\Lambda_0^2}{\Delta_{12}^2} - (-1)^{\deg f}\beta\,(t_1+t_2) \\ -\log\frac{\Lambda_0^2}{\Delta_{12}^2} - (-1)^{\deg f}\beta\,(t_1+t_2) & \log\left(t_2 \frac{\Delta_{12}^2}{\Lambda_0^2}\right) + \gamma t_2 + \beta t_1 \end{bmatrix} \tag{B.8}$$

$$\begin{bmatrix} 2\pi i\mathcal{F}_{111} & 2\pi i\mathcal{F}_{112} \\ 2\pi i\mathcal{F}_{122} & 2\pi i\mathcal{F}_{222} \end{bmatrix} = \begin{bmatrix} \frac{1}{g\Delta_{12}^3 f(a_1)}\left(\frac{1}{t_1}+\gamma\right) & \frac{-\beta}{g\Delta_{12}^3 f(a_2)} \\ \frac{\beta}{g\Delta_{12}^3 f(a_1)} & \frac{-1}{g\Delta_{12}^3 f(a_2)}\left(\frac{1}{t_2}+\gamma\right) \end{bmatrix} \tag{B.9}$$

where we have introduced the parameters:

$$\gamma = \left(2 + \frac{2\Delta_{12} f'(a_1)}{f(a_1)}\right)^2 - \Delta_{12}\frac{6f'(a_1) + 3\Delta_{12} f^{(2)}(a_1)}{2f(a_1)} \tag{B.10}$$

$$\beta = 4 + 6(-1)^{\deg f} + 4(-1)^{\deg f}\frac{\Delta_{12} f'(a_1)}{f(a_1)}. \tag{B.11}$$

References

[1] C. Vafa, *Superstrings and topological strings at large N*, *J. Math. Phys.* **42** (2001) 2798 [hep-th/0008142].

[2] S. Kachru, J. Pearson and H.L. Verlinde, *Brane/flux annihilation and the string dual of a non-supersymmetric field theory*, *JHEP* **06** (2002) 021 [hep-th/0112197].

[3] S. Kachru, R. Kallosh, A. Linde and S.P. Trivedi, *De Sitter vacua in string theory*, *Phys. Rev.* **D 68** (2003) 046005 [hep-th/0301240].

[4] S. Kachru and J. McGreevy, *Supersymmetric three-cycles and (super)symmetry breaking*, *Phys. Rev.* **D 61** (2000) 026001 [hep-th/9908135].

[5] R. Argurio, M. Bertolini, S. Franco and S. Kachru, *Gauge/gravity duality and meta-stable dynamical supersymmetry breaking*, *JHEP* **01** (2007) 083 [hep-th/0610212].

[6] M. Aganagic, C. Beem, J. Seo and C. Vafa, *Geometrically induced metastability and holography*, *Nucl. Phys.* **B 789** (2008) 382 [hep-th/0610249].

[7] H. Verlinde, *On metastable branes and a new type of magnetic monopole*, hep-th/0611069.

[8] J.J. Heckman, J. Seo and C. Vafa, *Phase structure of a brane/anti-brane system at large N*, *JHEP* **07** (2007) 073 [hep-th/0702077].

[9] R. Argurio, M. Bertolini, S. Franco and S. Kachru, *Metastable vacua and D-branes at the conifold*, *JHEP* **06** (2007) 017 [hep-th/0703236].

[10] S. Murthy, *On supersymmetry breaking in string theory from gauge theory in a throat*, *JHEP* **08** (2007) 013 [hep-th/0703237].

[11] J. Marsano, K. Papadodimas and M. Shigemori, *Nonsupersymmetric brane/antibrane configurations in type IIA and M theory*, *Nucl. Phys.* **B 789** (2008) 294 [arXiv:0705.0983].

[12] K. Intriligator, N. Seiberg and D. Shih, *Dynamical SUSY breaking in meta-stable vacua*, *JHEP* **04** (2006) 021 [hep-th/0602239].

JHEP04(2008)052

[13] H. Ooguri and Y. Ookouchi, *Meta-stable supersymmetry breaking vacua on intersecting branes*, *Phys. Lett.* **B 641** (2006) 323 [hep-th/0607183].

[14] S. Franco, I. Garcia-Etxebarria and A.M. Uranga, *Non-supersymmetric meta-stable vacua from brane configurations*, *JHEP* **01** (2007) 085 [hep-th/0607218].

[15] C. Ahn, *Brane configurations for nonsupersymmetric meta-stable vacua in SQCD with adjoint matter*, *Class. and Quant. Grav.* **24** (2007) 1359 [hep-th/0608160].

[16] I. Bena, E. Gorbatov, S. Hellerman, N. Seiberg and D. Shih, *A note on (meta)stable brane configurations in MQCD*, *JHEP* **11** (2006) 088 [hep-th/0608157].

[17] C. Ahn, *M theory lift of meta-stable brane configuration in symplectic and orthogonal gauge groups*, *Phys. Lett.* **B 647** (2007) 493 [hep-th/0610025].

[18] R. Tatar and B. Wetenhall, *Metastable vacua, geometrical engineering and MQCD transitions*, *JHEP* **02** (2007) 020 [hep-th/0611303].

[19] C. Ahn, *Meta-stable brane configuration with orientifold* 6 *plane*, *JHEP* **05** (2007) 053 [hep-th/0701145].

[20] C. Ahn, *More on meta-stable brane configuration*, *Class. and Quant. Grav.* **24** (2007) 3603 [hep-th/0702038].

[21] C. Ahn, *Meta-stable brane configuration and gauged flavor symmetry*, *Mod. Phys. Lett.* **A 22** (2007) 2329 [hep-th/0703015].

[22] A. Giveon and D. Kutasov, *Gauge symmetry and supersymmetry breaking from intersecting branes*, *Nucl. Phys.* **B 778** (2007) 129 [hep-th/0703135].

[23] C. Ahn, *Meta-stable brane configuration of product gauge groups*, *Class. and Quant. Grav.* **25** (2008) 075001 [arXiv:0704.0121].

[24] C. Ahn, *Meta-stable brane configurations with five* $NS5$*-branes*, arXiv:0705.0056.

[25] C. Ahn, *Meta-stable brane configurations by adding an orientifold-plane to Giveon-Kutasov*, *JHEP* **08** (2007) 021 [arXiv:0706.0042].

[26] C. Ahn, *More meta-stable brane configurations without* $D6$*-branes*, *Nucl. Phys.* **B 790** (2008) 281 [arXiv:0707.0092].

[27] R. Tatar and B. Wetenhall, *Metastable vacua and complex deformations*, *Phys. Rev.* **D 76** (2007) 126011 [arXiv:0707.2712].

[28] J.M. Maldacena, *The large N limit of superconformal field theories and supergravity*, *Adv. Theor. Math. Phys.* **2** (1998) 231 [*Int. J. Theor. Phys.* **38** (1999) 1113] [hep-th/9711200].

[29] S.S. Gubser, I.R. Klebanov and A.M. Polyakov, *Gauge theory correlators from non-critical string theory*, *Phys. Lett.* **B 428** (1998) 105 [hep-th/9802109].

[30] E. Witten, *Anti-de Sitter space and holography*, *Adv. Theor. Math. Phys.* **2** (1998) 253 [hep-th/9802150].

[31] I.R. Klebanov and M.J. Strassler, *Supergravity and a confining gauge theory: duality cascades and* χSB*-resolution of naked singularities*, *JHEP* **08** (2000) 052 [hep-th/0007191].

[32] J.M. Maldacena and C. Núñez, *Towards the large N limit of pure* $\mathcal{N} = 1$ *super Yang-Mills*, *Phys. Rev. Lett.* **86** (2001) 588 [hep-th/0008001].

JHEP04(2008)052

[33] R. Dijkgraaf and C. Vafa, *Matrix models, topological strings and supersymmetric gauge theories*, *Nucl. Phys.* **B 644** (2002) 3 [hep-th/0206255].

[34] R. Dijkgraaf and C. Vafa, *On geometry and matrix models*, *Nucl. Phys.* **B 644** (2002) 21 [hep-th/0207106].

[35] R. Dijkgraaf and C. Vafa, *A perturbative window into non-perturbative physics*, hep-th/0208048.

[36] R. Dijkgraaf, S. Gukov, V.A. Kazakov and C. Vafa, *Perturbative analysis of gauged matrix models*, *Phys. Rev.* **D 68** (2003) 045007 [hep-th/0210238].

[37] A.D. Shapere and C. Vafa, *BPS structure of Argyres-Douglas superconformal theories*, hep-th/9910182.

[38] M.R. Douglas, J. Shelton and G. Torroba, *Warping and supersymmetry breaking*, arXiv:0704.4001.

[39] F. Cachazo, K.A. Intriligator and C. Vafa, *A large N duality via a geometric transition*, *Nucl. Phys.* **B 603** (2001) 3 [hep-th/0103067].

[40] K. Intriligator, P. Kraus, A.V. Ryzhov, M. Shigemori and C. Vafa, *On low rank classical groups in string theory, gauge theory and matrix models*, *Nucl. Phys.* **B 682** (2004) 45 [hep-th/0311181].

[41] F. Cachazo and C. Vafa, $\mathcal{N} = 1$ *and* $\mathcal{N} = 2$ *geometry from fluxes*, hep-th/0206017.

JHEP04(2008)052